Master's Thesis

Design and Evaluation of a Customized and Body-powered Prosthesis using Fingertip Trajectories based on Polar Coordinate Analysis

Hyeonjun Kim

Department of Mechanical Engineering

Graduate School of UNIST

2019

Design and Evaluation of a Customized and Body-powered Prosthesis using Fingertip Trajectories based on Polar Coordinate Analysis

Hyeonjun Kim

Department of Mechanical Engineering

Graduate School of UNIST

Design and Evaluation of a Customized and Body-powered Prosthesis using Fingertip Trajectories based on Polar Coordinate Analysis

A thesis/dissertation
submitted to the Graduate School of UNIST
in partial fulfillment of the
requirements for the degree of
Master of Science

Hyeonjun Kim

12. 11. 2018

Approved by

Advisor
Joonbum Bae

Design and Evaluation of a Customized and Body-powered Prosthesis using Fingertip Trajectories based on Polar Coordinate Analysis

Hyeonjun Kim

This certifies that the thesis/dissertation of Hyeonjun Kim is approved.

12. 11. 2018

signature

Advisor: Joonbum Bae

signature

Gwanseob Shin

signature

Hyondong Oh

Abstract

This thesis presents a design and evaluation of a customized finger prosthesis that generates a natural finger motion. The design of the prosthesis followed two primary requirements: i) the size of the prosthesis should reflect that of an amputee's finger; ii) the prosthesis should enable the natural finger motion of the amputee. To achieve these aims, two methods were employed: i) an incomplete four-bar mechanism by utilizing the remaining joint of a subject as the joint in the mechanism; ii) a fingertip trajectory analysis in polar coordinates to model the natural finger motion as only one degree of freedom (DOF). A serially connected incomplete four-bar mechanism was applied to create an under-actuation system. The under-actuation system operated by a metacarpophalangeal (MCP) joint rotation of the amputee which makes proximal interphalangeal (PIP) and distal interphalangeal (DIP) joint rotations. The system does not need any actuators to control the two joint rotations, but employs the residuum of the amputee as an actuator.

The fingertip trajectory was considered as the typical factor to represent the natural finger motion, and a new curve fitting method in the polar coordinate of the fingertip trajectory was proposed. The method represents not only the finger motion of a single subject but also of people in general using the same order equation. To make the proposed mechanism move like the natural finger motion of the amputee, a fingertip trajectory curve from the curve fitting method was used as a reference for the mechanism in an optimization process. During the optimization process, the design variables were chosen by considering data from the finger amputee (e.g. residuum size, expected phalangeal lengths, etc.) as well as the requirements of the finger prosthesis.

A modular wearable interface was proposed to allow the system to be worn easily and the system joint to be manually aligned to the finger joint accurately. As we focused on the design of the finger prosthesis, the prototype was manufactured based on the finger information of a normal subject before applying it to the actual finger amputee. The performance of the proposed system was verified by intensive experiments for grasping and manipulation while wearing the proposed system.

Contents

List of Figures

List of Tables

I. Introduction

About 541,000 people became upper limb amputees in 2005 in the United States and the number of amputees will be at least double by 2050, as shown in Fig. I.1 [1]. The three main reasons of amputation are vascular disease including diabetes and peripheral arterial disease, trauma and cancer [1]. According to the Healthcare Cost and Utilization Project (HCUP-NIS), the number of finger amputees occupied about 80% of the total upper limb amputations as shown in Fig. I.2 [2]. Finger amputation affects the ability to perform daily living, working and social activities of amputees [1, 3]. Hence, recovering the function of the finger is important to get back to social and/or working environments. One of the ways to restore finger function is the use of prostheses that helps amputees grasp objects.

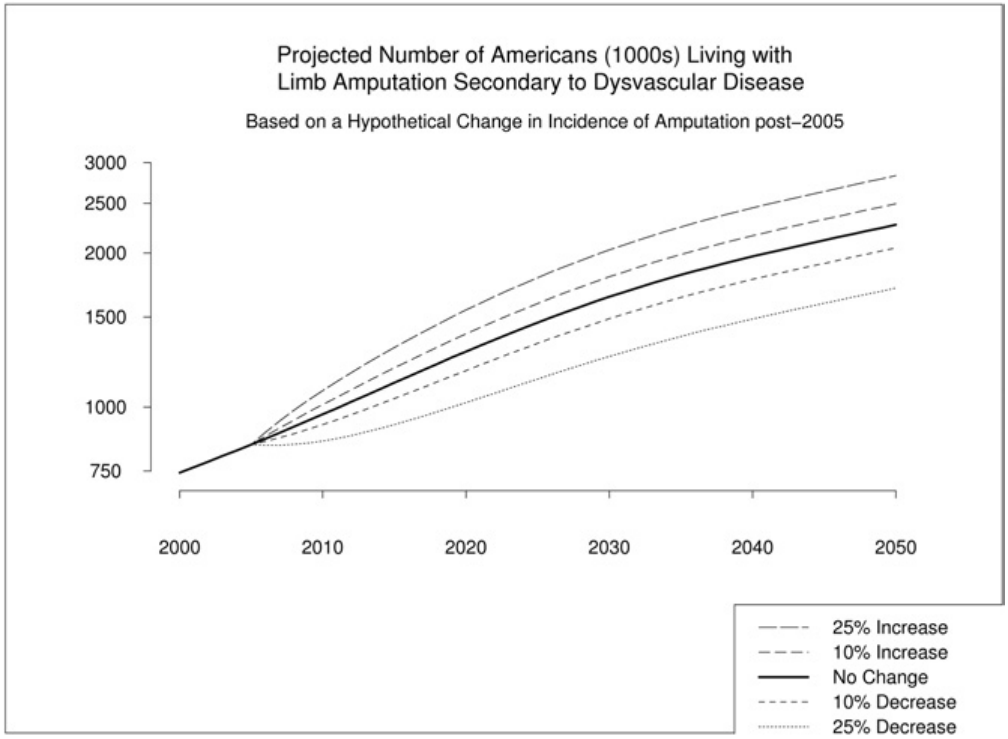

Fig. I.1 Projected number of Americans living with limb amputation secondary to dysvascular disease (log scale) from year 2000 to 2050 [1]

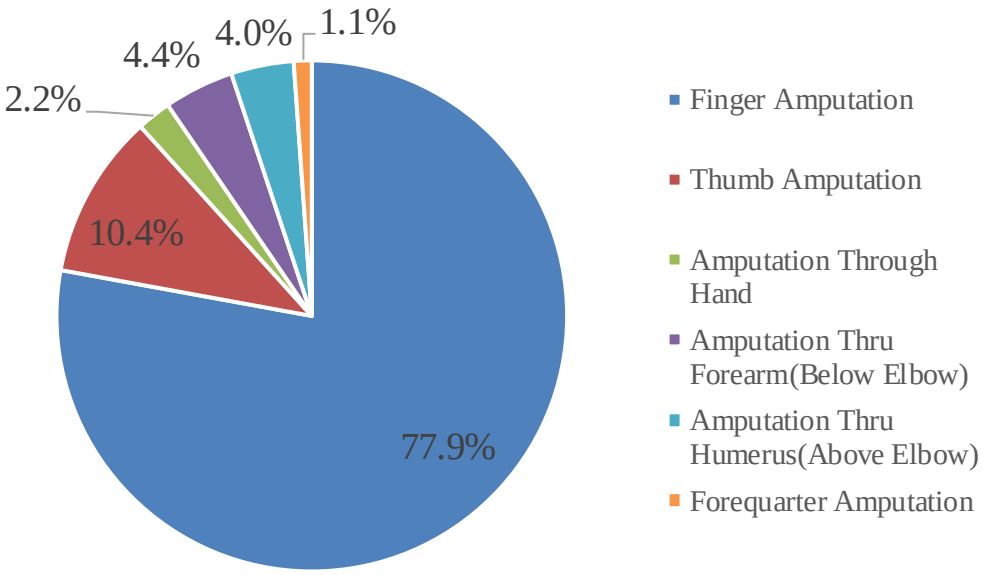

Fig. I.2 Portion of upper limb amputation [2]

Prostheses have been used throughout history. The wooden toe found on the body of on ancient Egyptian is the first known concept of the prostheses as shown in Fig. I.3 (a) [4]. These kinds of prostheses did not have joints, which means that prostheses had very limited functionality, however, in the early sixteenth century, a doctor, Ambroise Paré, introduced a hinged hand and leg with a knee joint prosthesis, which gave more functionality to the amputee than the previous wooden prostheses as shown in Fig. I.3 (b) [5]. Even though the functionality was already considered and applied, the prostheses are not common nowadays because of complex requirements of the prostheses to be chosen by the amputees.

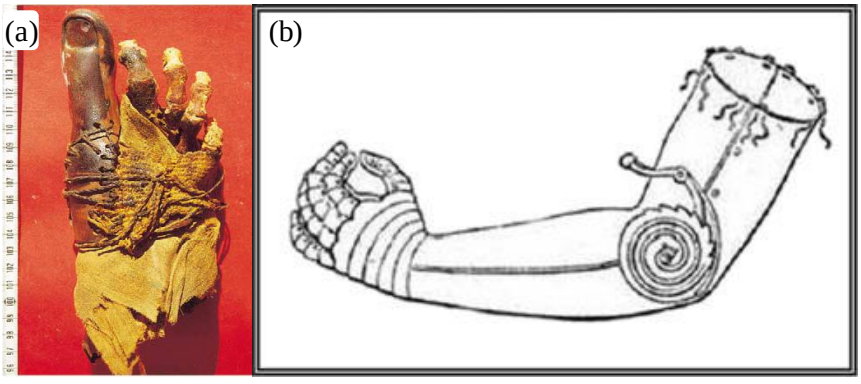

Fig. I.3 The early history of artificial limbs

(a) an ancient wooden toe prosthesis [4] and (b) a functional prosthesis with a hinged hand [5]

Most prostheses have not given satisfaction and even have been abandoned because of the complex requirements of the prostheses: unappealing appearance, limited performance and fitting. The

appearance of the prostheses is important to the amputees because they do not want attention from other people. Even if the prostheses have a dexterous function or performance, the amputees will not choose the prostheses if the prostheses have a strange appearance. The performance of the prostheses is also the consideration for the amputee to achieve a vocational and recreational purpose. Lastly, taking into account the fitting of the prostheses helps the amputees use the prostheses for a long time. To deal with that, many finger prostheses of various mechanisms have been researched to improve the quality of life of the finger amputees [6-12], and the state of the art of the finger prostheses is discussed in the next section.

In this thesis, because we focused on the design method of the finger prosthesis, the prototype was manufactured using the information of a normal subject, and was verified by the trajectory generation and the grasping performance experimentally before applying it to an actual finger amputee. Although the information of the normal subject was used to design the prosthesis, the design method can be consistently applied when the actual information of the finger amputee is acquired. Therefore, we describe the proposed design method as we assume to use the information of the finger amputee.

The remainder of this thesis is organized as follows. After discussing hand anatomy and requirements of the system in Section II, we propose a design process of the proposed prosthesis in Section III.1. In particular, the finger motion measurement system is discussed in Section III.1.4. Performance is verified by simulations and experiments in Section III.2. Finally, the conclusions and futures work are summarized in Section IV.

II. Configuration of the Functional Finger Prosthesis

II.1 Muscular-skeletal Structures of the Finger

The finger prosthesis is the device that replaces the amputated finger and supports the finger motion to grasp and manipulate an object or some motions of ADL. Therefore, an understanding of biomechanical characteristics of the fingers is significant to develop the finger prosthesis. The thumb has three bones of a metacarpal phalanx (MP), a proximal phalanx (PP) and a distal phalanx (DP) and three joints of carpometacarpal (CMC), metacarpophalangeal (MCP) and interphalangeal (IP) joints. Other fingers have three bones of the proximal phalanx (PP), an intermediate phalanx (IP) and a distal phalanx (DP), and three joints of metacarpophalangeal (MCP), proximal interphalangeal (PIP), and distal interphalangeal (DIP) joint [13]. The IP joints, including the PIP and DIP joints, have one degree of freedom (DOF) for the flexion/extension (F/E), and the MCP joint and CMC joint have two DOFs for the flexion/extension (F/E) and abduction/adduction (A/A). Therefore, each finger without thumb has four DOFs, however, when it comes to the grasping motion, the F/E motion of the fingers generally outweighs the A/A motion of the fingers [14].

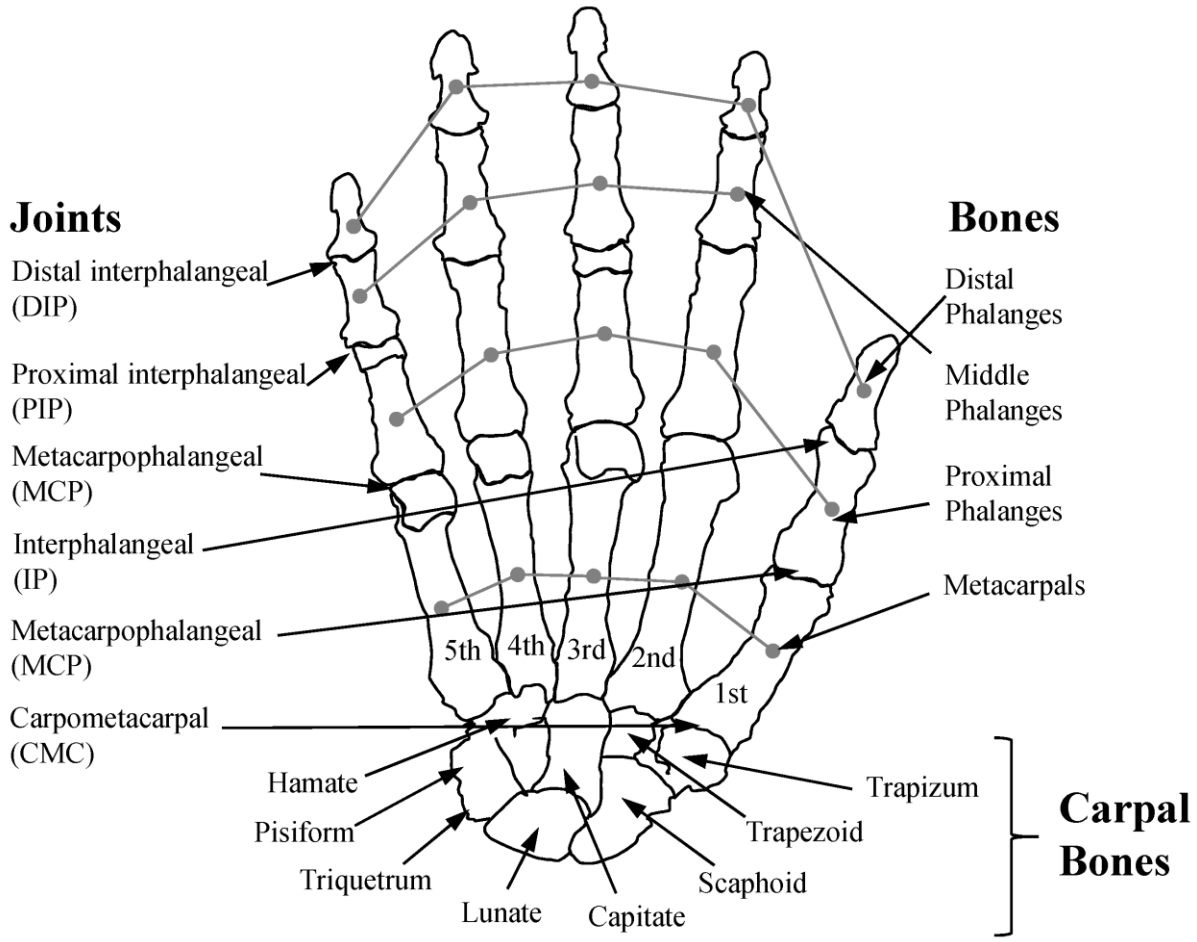

Fig. II.1 Skeletal structure of the human hand [15]

Fingers have a large workspace; the normal range of motion (ROM) of the MCP, PIP and DIP joints are about 0 ~ 100˚, 0 ~ 105˚ and 0 ~ 85˚, respectively [16]. However, people usually using specific ROM during the ADL, called functional ROM; that of the MCP, PIP and DIP joints are about 33 ~ 73˚, 36 ~ 86˚ and 20 ~ 61˚, respectively [16]. Various ROMs can be applied to the finger device depending on the targeted range of the finger motion.

	MCP	**PIP**	**DIP**
Normal ROM	0~100º	0~105º	0~85º
Functional ROM	33~73º	36~86º	20~61º

Table II.1 Human finger range of motion [16]

II.2 Requirements of the System

II.2.1 *The State of the Art*

Finger prostheses are classified into three types in terms of actuation mechanism: a non-functional prosthesis, an external-powered prosthesis and a body-powered prosthesis. First, the non-functional prostheses have been usually made by silicone to complement the aesthetic part of the amputee, resulting that it has few functional roles to grasp or manipulate an object [6]. The external-powered prostheses are the systems that use actuators to move fingers through an external power source or a battery. I-digits quantum (Touch bionics [7]) in Fig. II.1 (e) is one of the external-powered prostheses, which uses two actuators per finger to move MCP joint and PIP joint. The system is developed for a partial hand amputee and is bulky and heavy because of the peripheral including the battery.

The body-powered prostheses in Fig. II.1 (b), (c) and (d) are the prostheses actuated by the patient's residuum as a power source. According to the transmission methods, they are divided into cable-driven and linkage type [8-10]. The cable-driven devices utilize the cable to flex the finger structure along with the movement of the finger residuum and usually use a return spring to maintain the tension of the spring. M-finger in Fig. II.1 (b) uses the movement of MCP joint as a power source, the structure rotates as the cable are extended during amputee's flexion and the return spring pulls the cable during the amputee's extension motion. The cable-driven devices can be compact by the thin and flexible characteristics of the cable. But the durability is lower than that of the linkage type device because the cable in the device can be loosened or even broken [11]. Also, most cable-driven devices are designed to follow a simple circular trajectory which only one joint rotates, and other joints are fixed, rather than a trajectory which multiple joints rotates together.

On the other hand, the linkage type devices utilize the rigid linkage mechanism (e.g., a four-bar mechanism) to make the multiple joints rotation. The linkage mechanism can create various angle trajectories of input and output links by adjusting the link combinations. The x-finger [9] and MCP

driver [10] use four-bar linkage mechanism to realize the natural finger motion as the patient's MCP joint rotates. The linkage type devices have high durability and can make various finger trajectories according to the link combination. However, the structure can be bulkier than the cable driven structure [12].

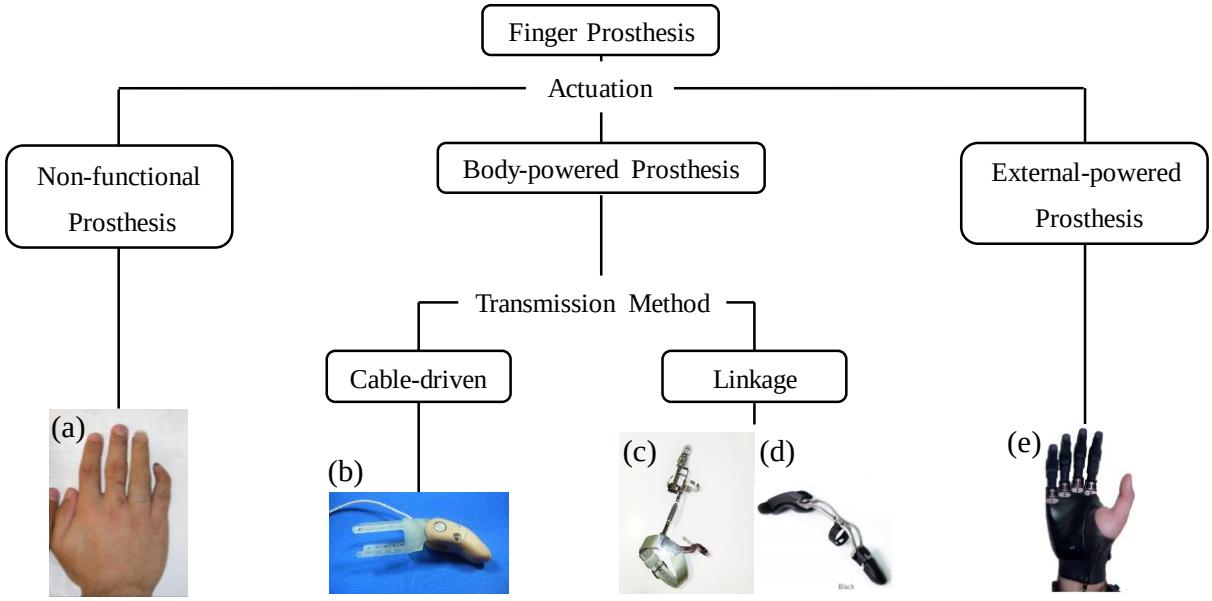

Fig. II.2 Prostheses state of the art

II.2.1 *Target Objectives*

Even though many systems by the various actuation mechanisms have been developed, there are few devices to enable the patient to perform the activities of daily living (ADL) naturally and satisfy the design with respect to the aesthetic sense. The requirements for the practical finger prosthesis are as follows;

1) The prosthesis should move various joints simultaneously without exceeding the amputee's finger size,

2) the prosthesis help grasp and manipulate the objects by the natural finger motion, and

3) the prosthesis is fitted well to the hand of the patient.

In this thesis, a design method of a body-powered finger prosthesis by considering those requirements are proposed. The proposed system has four characteristics accordingly:

1) serially connected incomplete four-bar mechanisms not to exceed the finger size,

2) natural finger motion analysis based on the fingertip trajectory in polar coordinate,

3) optimization process to customize the link lengths for the finger sized prosthesis realizing the natural finger motion, and

4) modular wearable interface to easily wear the proposed system preventing the whole system from re-wearing to align the joint location.

III. Design Process and Experimental Verification

The proposed prototype is shown in Fig. II.3. In this thesis, the targeted user is the patient whose proximal phalanx of the index finger is amputated. Hence, the proposed structure is implemented as an under-actuation mechanism in which the PIP and DIP joints rotates depending on the remained MCP joint movement of the patient. The under-actuation mechanism includes two consecutive 4 bar mechanisms; in order to reduce the prosthesis size, the incomplete four-bar mechanism using the residuum as a link of four-bar mechanism and the bent link in the first four-bar mechanism, which makes first and second four-bar mechanism (i.e, PIP and DIP joint movements) rotate in the same way, is applied. Details of the design will be discussed in the next section.

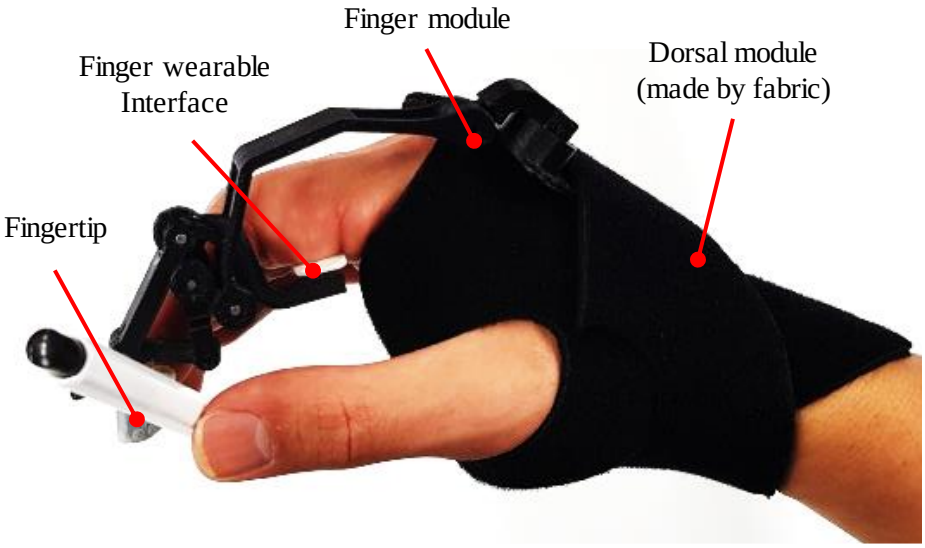

Fig. II.3 Proposed system

The finger module is made of ABS material through a 3D printing technique based on the result of the link lengths derived from the optimization. The end-effector is made in a shape like the human fingertip by silicon material, which is deformed adaptatively to the various object shapes so that it can hold and manipulate the object better.

The wearable parts of the proposed system consist of a dorsal module and a finger module as shown in Fig. II.3. They can be worn separately and then combined by the Velcro. The dorsal module is made of fabric and fixed by inserting the thumb into the hole of the module and covering the overall dorsum of the hand. The finger module is fixed to the finger as the structure is located under the residuum and the urethane belt connects the structure and the residuum of the finger. Finally, the dorsal part of the finger module is attached on the dorsal module by using the Velcro.

III.1 Design Process

III.1.1 Design Flow

Our prosthesis is designed in the order of Fig. III.1. The process is divided into the finger module and the dorsum module, and each module has the wearable interface. First, we chose 1 DOF under-actuation mechanism among various candidates for the finger module and measured the amputee's anthropometry data including both amputated and undamaged fingers including ROM, each joint angle and trajectories for the customization. After that, cost function criteria were defined for the optimization of the mechanism to make natural finger motion. The wearable interface including dorsum module designed considering the swelling phenomenon residuum.

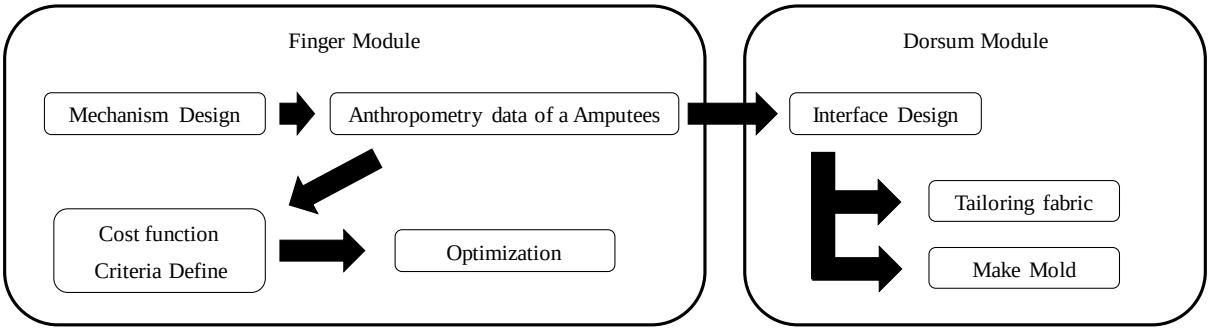

Fig. III.1 A series of design flow chart

III.1.2 Mechanism Design

In this section, the mechanism design process and the final design of the proposed system are discussed. The proposed system is designed by the following considerations. First, the system should be under-actuated, which makes two joint movements simultaneously through the other joint rotation. That is, the MCP joint rotation makes the PIP and DIP joint movements. Second, the ROM of the PIP and DIP joint should have similar the ROM of human joints in order to realize natural flexion/extension motion. Lastly, the size of the system should not exceed the human finger size from an aesthetic point of view.

Various mechanisms can be used for the first consideration (under-actuation), however, the linkage mechanism (i.e., serially connected four-bar mechanism) is chosen for the higher durability than that of the cable-driven mechanism. The second consideration (natural flexion/extension motion) is satisfied by selecting appropriate four-bar mechanism type according to the rotation direction of each joint among various four-bar mechanism types.

Fig. III.2 shows two basic types of four-bar mechanism: (a) a basic four-bar mechanism type with a trapezoidal shape and (b) an X-shaped four-bar mechanism. The dashed lines and solid lines are when the angle of the MCP joint is 0˚ and when the MCP joint is flexed, respectively, and the black dot shows the trajectories of the IP. The two types of four-bar mechanism show different rotation direction of the

PIP joint according to a counter-clockwise rotation of the MCP joint; the PIP joint is rotated in a reverse direction (clockwise) at the basic four bar mechanism type as shown in Fig. III.2 (a) and the same direction (counter-clockwise) at the X-shaped four-bar mechanism type as shown in Fig. III.2 (b). The rotation direction of the MCP and PIP joints must be same to make the natural flexion/extension motion through the under-actuation mechanism, so that the X-shaped four-bar mechanism is applied to the first four-bar mechanism to satisfy the second condition (natural flexion/extension motions). The operation according to the MCP joint angle (θ_{MCP}) is shown in Fig. III.3.

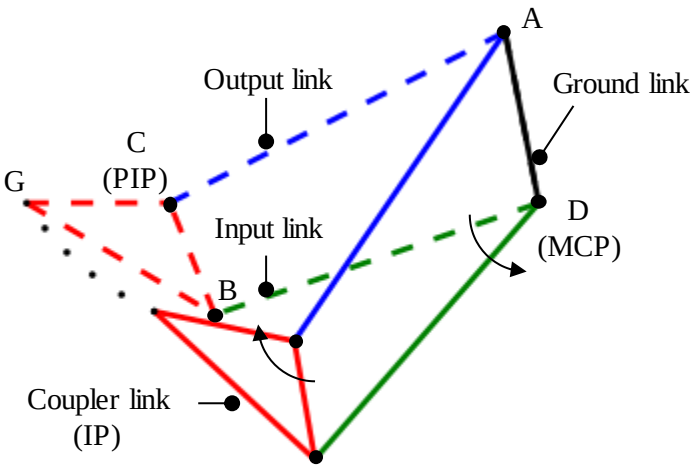

(a) A basic four-bar mechanism

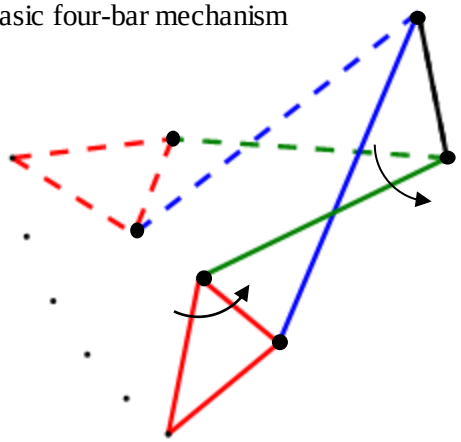

(b) An X-shape four-bar mechanism

Fig. III.2 Basic concepts of 4 bar mechanism

(a) General 4 bar (b) X-shape 4 bar

where r_1 and r_2 are input link length, and g is ground link length. θ and ψ are input and output angles respectively.

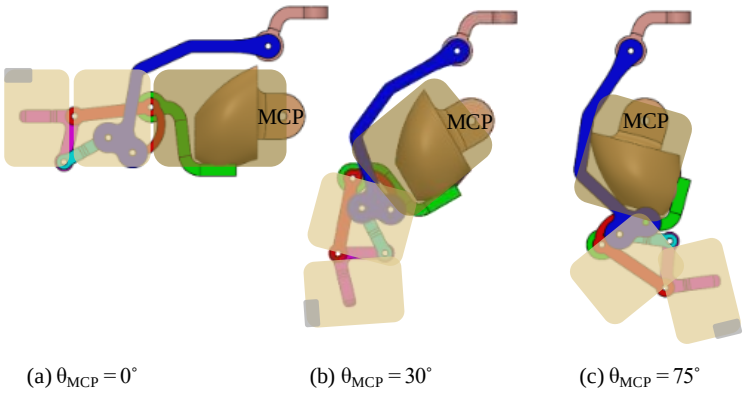

Fig. III.3 Operation of the proposed system

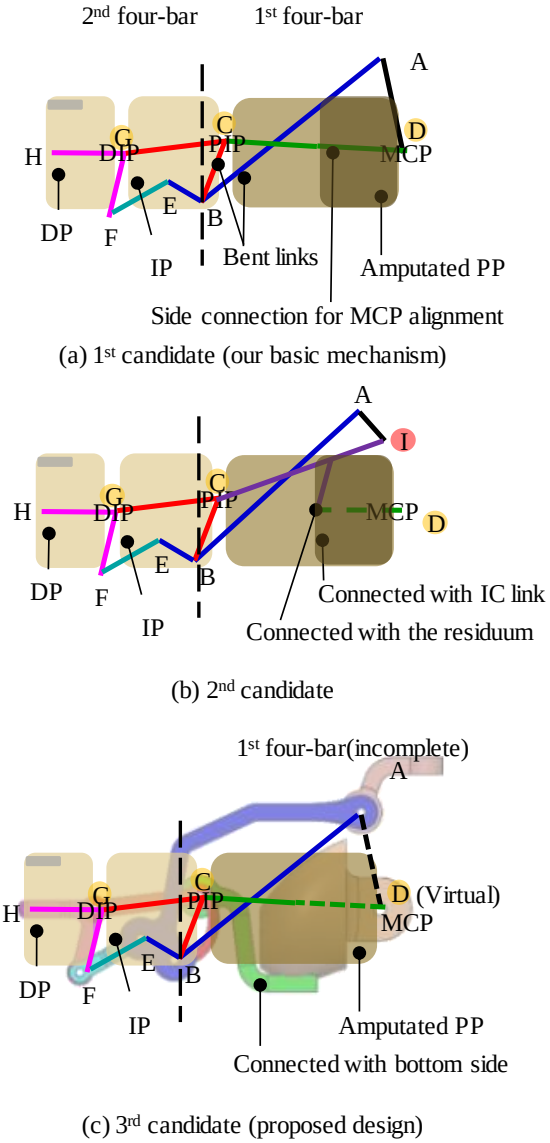

Fig. III.4 Design candidates and final design of the proposed system (a) first version (b) second version (c) proposed(final) version system

Also, the bent links (GCB and ABE link in Fig. III.4 (a)) are applied to satisfy the natural finger motion. At first, if the basic four-bar mechanism (GCBF link in Fig. III.4 (a)) is serially connected without the bent link, the total DOF of the device is two, resulting that the proposed system is not the under-actuation system. Therefore, the two bent links are applied to couple the two four-bar mechanism as one DOF. We design the first bent link of GCB link and consider whether the other bent link should be output link (CD link) or input link (AB) to satisfy above design considerations. If the output (CD) link becomes the bent link such as ABE link in Fig. III.4 (a), the bent link rotates by exceeding the finger size (i.e., outside from CG link) during the MCP joint rotation. On the other hand, the proposed ABE bent link is always in the finger size range since the BE link rotates clockwise, which makes the two four-bar mechanism rotate in the same way. And, ROM of PIP and DIP joints of the system can be easily adjusted by changing the length and the angle of the bent link in the proposed mechanism.

Taking into the above three considerations account, three design candidates were considered as shown in Fig. III.4. The first design candidate in Fig. III.4 (a) was that the CD link was located beside the PP and the MCP joint. This design was difficult to match D joint with the amputee's MCP joint and could not be applied to the middle and ring fingers where the structure could not be located beside the MCP joint.

The second design was considered not to locate CD link at the side of the MCP joint. A new I joint was added under the A joint and new IC link was connected to the finger wearable interface of the MCP joint as shown in Fig. III.4 (b). It could be applied to the middle and ring fingers due to the different joint matching location from the side to the upper of the MCP joint. However, kinematically, input and output angle range in the first four-bar mechanism was smaller than the actual ROM of MCP and PIP joints. The process to obtain the θ_I according to the MCP joint angle (θ_{MCP}) is as follows.

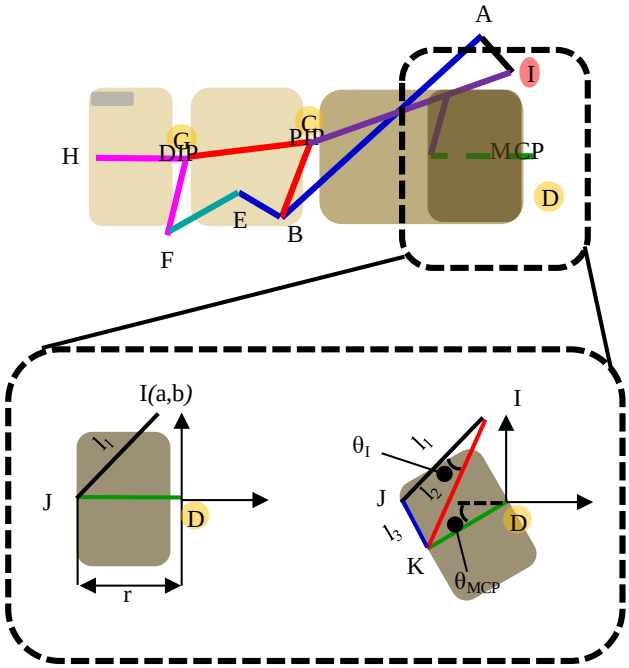

Fig. III.5 I joint force effect analysis

J and K point are initial and last position of the residuum, respectively, and l_1, l_2 and l_3 are length of IJ, IK and IK links, respectively.

The vector DK can is expressed as follow:

$$\overrightarrow{DK} = [-r\cos(\theta_{MCP}), -r\sin(\theta_{MCP})] \tag{III.1}$$

And the MCP joint angle (θ_I) is expressed by law of cosines:

$$\theta_I(\theta_{MCP}) = \arccos\left(\frac{l_1^2 + l_2(\theta_{MCP})^2 - l_3(\theta_{MCP})^2}{2l_1 l_2(\theta_{MCP})}\right) \tag{III.2}$$

where $l_1 = \left\|\overrightarrow{DJ}\right\| = \sqrt{(a+r)^2 + b^2}$, $l_2(\theta_{MCP}) = \left\|\overrightarrow{IK}\right\| = \sqrt{\left|a + r\cos(\theta_{MCP})\right|^2 + \left|b + r\sin(\theta_{MCP})\right|^2}$ and

$l_3(\theta_{MCP}) = \left\|\overrightarrow{JK}\right\| = r\sqrt{\left(\sin(\theta_{MCP})\right)^2 + \left(\left(\cos(\theta_{MCP}) - 1\right)\right)^2}$

The analytical result, (III.2) is hard to know the relationship intuitively, therefore, the simulation is conducted with various value set. The b value is chosen as 10 which can be the smallest value because of the dorsal bone. The black line means that the I joint is same as the D (MCP) joint, so that the two angles are also same. However, the angle of the I joint (θ_I) is smaller than the MCP joint (θ_{MCP}). In the first four-bar mechanism of the second candidate, the angle of the I joint (θ_I) is the input link, that is the ROM of the second system is smaller than the other candidates.

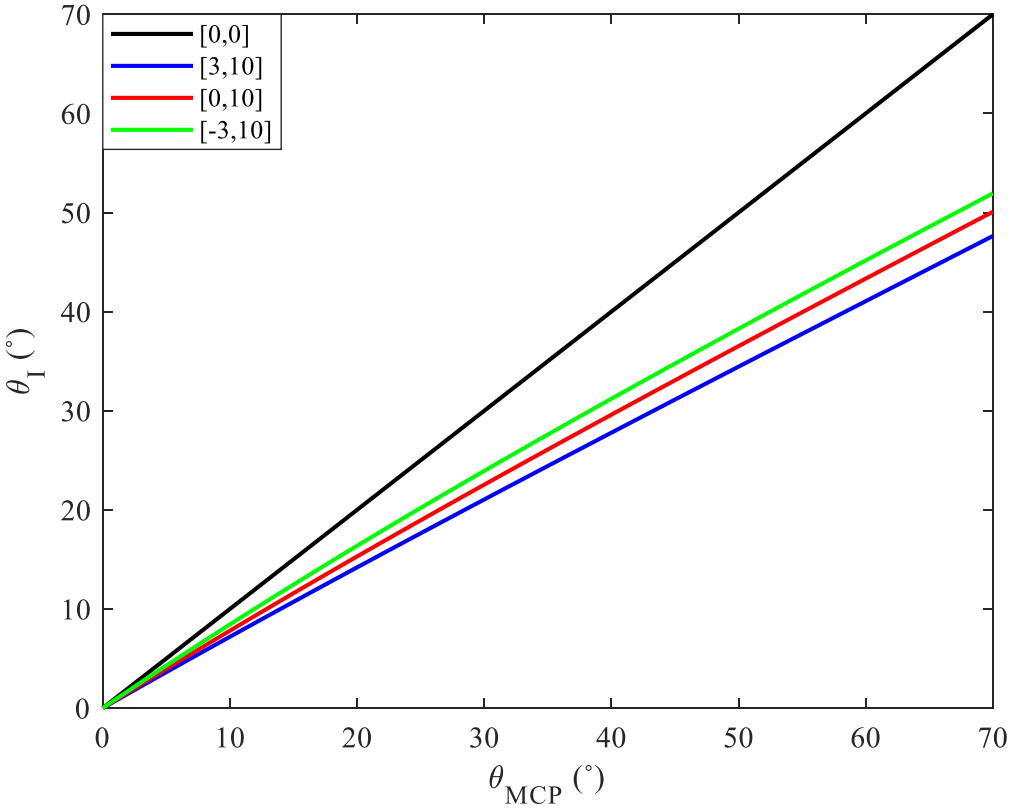

Fig. III.6 I joint angle according to the MCP joint angle

a and b are 0 and 0 in the black line, 3 and 10 in the blue line, 0 and 10 in the red line, and -3 and 10 in the green line, respectively.

Moreover, the I joint generates the force applied to the residuum, which makes the wearable interface wobble. Because the I and D joint have the different center of rotation as shown in Fig. III.5 which is detail view of the Fig. III.4 (b). It means that strain (the difference between l_1 and l_2) occurs when the residuum rotates. The process to obtain the force according to the MCP joint angle (θ_{MCP}) is as follows.

The force is expressed by Hook's law:

$$F(\theta_{MCP}) = \frac{\vec{\delta}(\theta_{MCP})EA}{l_1} \tag{III.3}$$

where $\vec{\delta}(\theta_{MCP}) = \vec{l_2}(\theta_{MCP}) - l_1$

$$= \sqrt{\left|a + r\cos\left(\theta_{\mathrm{MCP}}\right)\right|^2 + \left|b + r\sin\left(\theta_{\mathrm{MCP}}\right)\right|^2} - \sqrt{\left|a + r\right|^2 + \left|b\right|^2}$$

$= r\sqrt{2(1-\cos\theta_{MCP})} - \sqrt{|a+r|^2 + |b|^2}$ and E and A are Young's modulus and cross-sectional area of the structure material, respectively.

Because of the I joint, the unnecessary force is applied to the residuum, and it will make the amputee feel uncomfortable and even the system inaccurate.

Finally, the proposed system was designed as shown in Fig. III.4 (c); the amputee's MCP joint was assumed as the virtual D joint in the first four-bar mechanism and the residuum was connected to the structure so that it was acted as CD link. This design could be applied to other fingers because the structure was connected to the bottom of the PP and was compact than the previous design candidates by utilizing the virtual D joint. It may be difficult to match D joint and actual MCP joint, but it could be overcome by the modular wearable interface which could adjust the location of the proposed device manually. The details of wearable method will be explained in the next section.

III.1.3 Kinematic Analysis

Fig. III.7 shows link lengths and angles for kinematic analysis. The joints and link lengths are expressed in upper cases and in lower cases, respectively. θ_1 to θ_4 are the angles relative to the x-axis, respectively. In particular, φ_2 is the BE link angle and φ_3 is the virtual link BG angle.

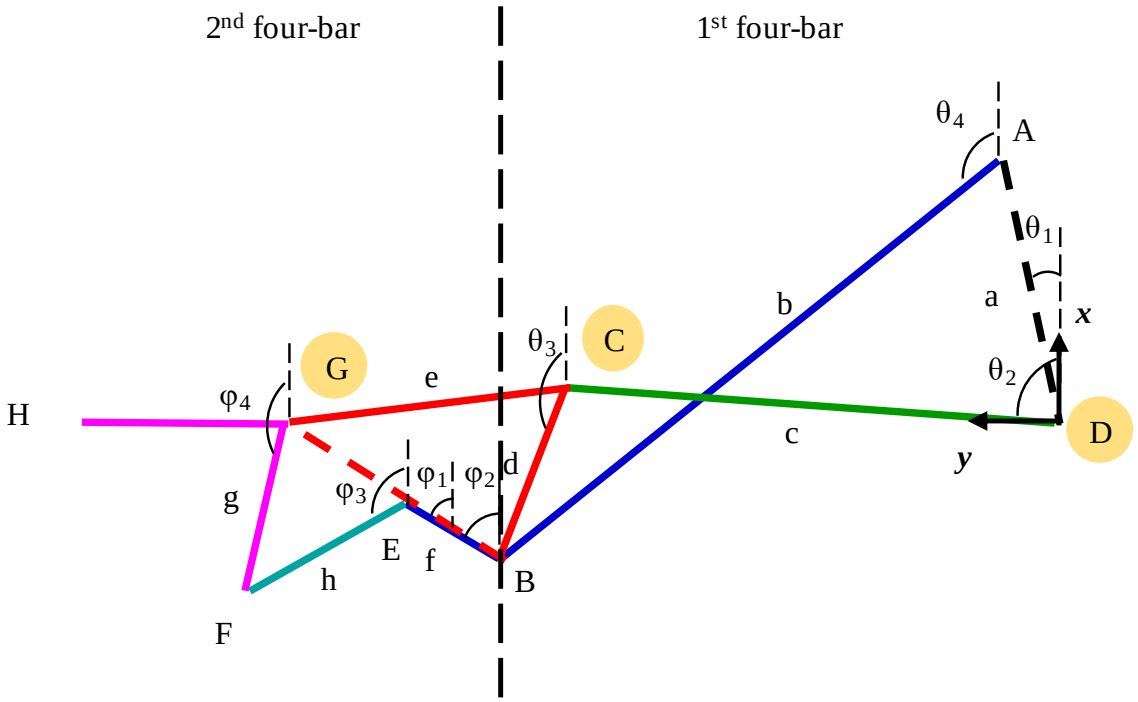

Fig. III.7 Link and angle parameters for kinematic analysis

A~G: Joint, H: Fingertip, $a \sim h$: Link length, θ_1: Fixed angle θ_2: Input angle (MCP), θ_3, θ_4 and φ: dependent angle

The process to obtain the PIP joint angle (θ_3) and the DIP joint angle (φ_4) according to the MCP joint angle (θ_2) is as follows.

First four-bar mechanism is expressed in Euler equation:

$$\overrightarrow{DA} - \overrightarrow{DC}(\overrightarrow{CA}) = \overrightarrow{CB} - \overrightarrow{AB}(\overrightarrow{CA}) \quad \text{(III.4)}$$

$$ae^{i\theta_1} - ce^{i\theta_2} = de^{i\theta_3} - be^{i\theta_4} \quad \text{(III.5)}$$

where a, c, d and b are the link lengths in Fig. III.7.

By dividing into x and y axis,

(III.5) can be rewritten as:

$$\cos\theta_3 = \frac{x + b\cos\theta_4}{d}, \sin\theta_3 = \frac{y + b\sin\theta_4}{d} \quad \text{(III.6)}$$

where $x = a\cos\theta_1 - b\cos\theta_2$, $y = a\sin\theta_1 - b\sin\theta_2$.

Pythagorean identity is applied to (III.6):

$$\left(\frac{x+b\cos\theta_4}{d}\right)^2+\left(\frac{y+b\sin\theta_4}{d}\right)^2=1$$

$$\rightarrow \frac{x^2+2bx\cos\theta_4+b^2(\cos^2\theta_3+\sin^2\theta_3)+y^2+2by\sin\theta_4}{d^2}=1$$

$$\rightarrow x\cos\theta_4+y\sin\theta_4=\frac{d^2-x^2-y^2-b^2}{2b} \quad \text{(III.7)}$$

The left side of (III.7) also can be expressed by cosine subtraction formula:

$$x\cos\theta_4+y\sin\theta_4=\sqrt{x^2+y^2}\cos(\theta_4-\alpha) \quad \text{(III.8)}$$

where $\cos\alpha=\frac{x}{\sqrt{x^2+y^2}}$, $\sin\alpha=\frac{y}{\sqrt{x^2+y^2}}$.

By using (III.7) and (III.8), θ_4 is rewritten as:

$$\theta_4(\theta_2)=\arctan\left(\frac{a\sin\theta_1-c\sin\theta_2}{a\cos\theta_1-c\cos\theta_2}\right)\pm\arccos\left(\frac{d^2-a^2-c^2-b^2+2ac\cos(\theta_1-\theta_2)}{2b\sqrt{a^2+c^2-2ac\cos(\theta_1-\theta_2)}}\right) \quad \text{(III.9)}$$

By substituting (III.9) into (III.6), PIP joint angle (θ_3) is now rewritten as:

$$\theta_3(\theta_2)=\arccos\left(\frac{a\cos\theta_1-c\cos\theta_2+b\cos\theta_4}{d}\right) \quad \text{(III.10)}$$

DIP angle can get by applying second four-bar mechanism in a similar way:

Second four-bar mechanism is expressed in Euler equation:

$$\overrightarrow{BG}-\overrightarrow{BE}(\overrightarrow{EG})=\overrightarrow{BG}-\overrightarrow{BE}(\overrightarrow{EG}) \quad \text{(III.11)}$$

$$ee^{i\varphi_1}-fe^{i\varphi_2}=he^{i\varphi_3}-ge^{i\varphi_4} \quad \text{(III.12)}$$

where e, f, h and g are the link lengths in Fig. III.7. By dividing into x and y axis, (III.12) can be rewritten as:

$$\cos\varphi_3=\frac{x_2+g\cos\varphi_4}{h},\sin\varphi_3=\frac{y_2+g\sin\varphi_4}{h} \quad \text{(III.13)}$$

where $x_2=e\cos\varphi_1-f\cos\varphi_2$, $y_2=e\sin\varphi_3-f\sin\varphi_4$.

Pythagorean identity is applied to (III.13):

$$\left(\frac{x_2+g\cos\varphi_4}{h}\right)^2+\left(\frac{y_2+g\sin\varphi_4}{h}\right)^2=1$$

$$\rightarrow \frac{{x_2}^2+2gx_2\cos\varphi_4+g^2(\cos^2\varphi_3+\sin^2\varphi_3)+{y_2}^2+2gy_2\sin\varphi_4}{h^2}=1$$

$$\rightarrow x_2\cos\varphi_4+y_2\sin\varphi_4=\frac{h^2-{x_2}^2-{y_2}^2-g^2}{2g} \quad \text{(III.14)}$$

The left side of (III.14) also can be expressed by cosine subtraction formula:

$$x_2 \cos\varphi_4 + y_2 \sin\varphi_4 = \sqrt{x_2^{\,2} + y_2^{\,2}} \cos(\theta_4 - \beta) \tag{III.15}$$

where $\cos\beta = \dfrac{x_2}{\sqrt{x_2^{\,2} + y_2^{\,2}}}$, $\sin\beta = \dfrac{y_2}{\sqrt{x_2^{\,2} + y_2^{\,2}}}$.

By using (III.14) and (III.15), φ_4 is rewritten as:

$$\varphi_4(\theta_2) = \arctan\left(\frac{e\sin\left(\theta_{\text{cbg}} + \theta_3(\theta_2)\right) - f\sin\left(\theta_{\text{abe}} + \theta_4(\theta_2)\right)}{e\cos\left(\theta_{\text{cbg}} + \theta_3(\theta_2)\right) - f\cos\left(\theta_{\text{abe}} + \theta_4(\theta_2)\right)}\right) \pm \arccos\left(\frac{\beta + f^2 + g^2 - h^2}{2g\sqrt{\beta + f^2}}\right) \tag{III.16}$$

where e, f, g and h are the link lengths θ_{cbg} and θ_{abe} are fixed angles in Fig. III.7, $\varphi_1 = \theta_{cbg} - (\pi - \theta_3(\theta_2))$, $\varphi_2 = \theta_{abe} - (\pi - \theta_4(\theta_2))$ and $\beta = e^2 - 2\cos\left(\theta_{\text{abe}} - \theta_{\text{cbg}} - \theta_3(\theta_2) + \theta_4(\theta_2)\right)ef$.

By kinematic analysis, the DIP and PIP joint angles (φ_4 and θ_3) are expressed in terms of the MCP joint angle (θ_2), which is consistent with the proposed under-actuation system. The obtained joint angles will be used to the optimization process which will be discussed in the next section.

III.1.4 Analysis of Finger Motion

III.1.4.1 Finger Motion Measurement Device

As previously mentioned, each finger has four DOFs, three F/E and one A/A, therefore, to measure finger motion is needed three actuators without A/A motion. As shown Fig. III.8, Various methods were developed to measure finger movement [17-23]. These systems can be classified as desktop systems and portable systems. The desktop systems shown in Fig. III.8 (a) and (b) typically need the equipment such as cameras with the reflective markers and space to measure even though the systems are accurate. In contrast, portable systems have more mobility and don't need additional peripherals. CyberGlove as shown in Fig. III.8 (c) is highly used in the commercial market, however, this product has limited accuracy because of the modified anatomical model [19]. And the soft material-based systems as shown in Fig. III.8 (d) and (e) have low interference when a user flexes his/her fingers. But these systems don't measure the DIP joint angle of the fingers, therefore, only measure natural grasp posture [22]. Plus, they have the hysteresis error due to the soft material, which affects system accuracy. The cable-mechanism system using the potentiometer as shown in Fig. III.8 (f) also showed low accuracy at the DIP angle because the system did not measure the DIP joint angle of the finger directly. Moreover, our finger motion experiment showed that the PIP and DIP have different ratio between each individual (0.5 ~ 0.8) as shown in Fig. III.9. Although the system as shown in Fig. III.8 (g) measures the DIP joint angle among these portable systems, the system only measures index finger of the person because of the MCP joint measuring method. The characteristics of these systems are compared in Table III.1.

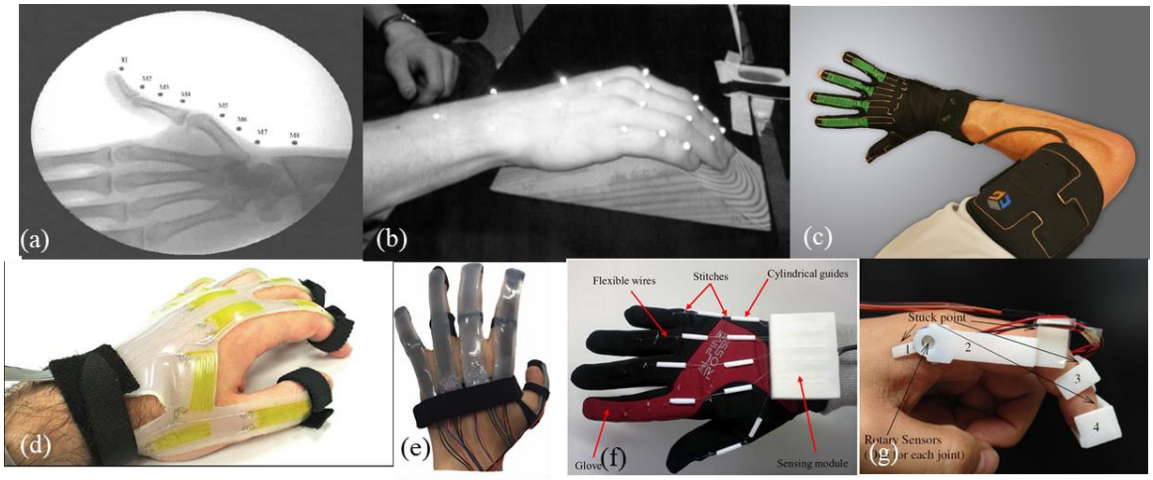

Fig. III.8 Previously developed finger motion measurement systems

(a) 2D fluoroscopy method[17]; (b) IR camera based method [18]; (c) CyberGlove [19]; (d)Wearable soft artificial skin [20]; (e) Soft sensor glove using E-Gain [21]; (f) Potentiometer-based system [22]; (g) Rotary sensor-based system [23]

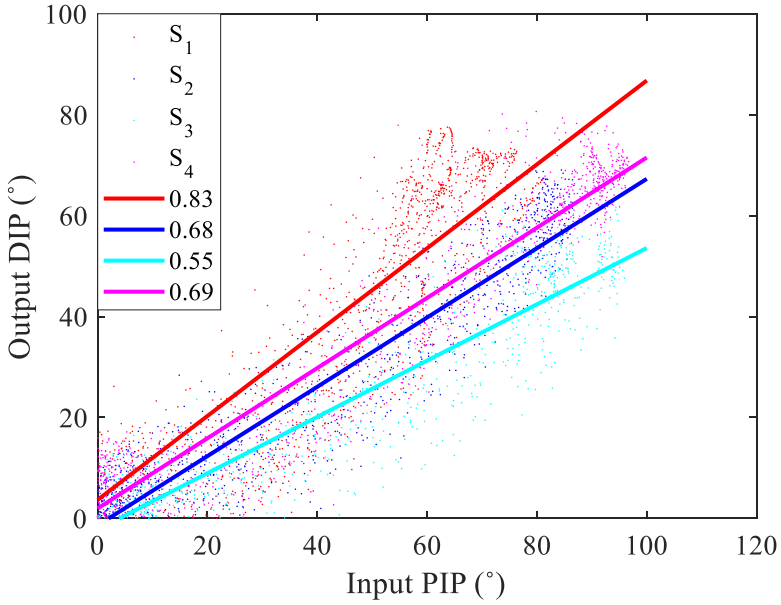

Fig. III.9 PIP and DIP joints relationships (four subjects)

	Type	Portability	Accuracy	Measuring DIP joint directly	Measuring point
(a)	Fluoroscopy (real time X-ray)	X	NA (High)	O	Fingers and Thumb
(b)	Mocap with marker	X	NA (High)	O	Fingers and Thumb
(c)	Flex sensor	O	Middle (3˚)	X	Fingers and Thumb
(d)	Soft sensor	O	NA	X	Fingers and Thumb
(e)	Soft sensor	O	Middle (3˚)	X	Fingers and Thumb
(f)	Potentiometer with cable mechanism	O	Low (6˚) at DIP joint	X	Fingers and Thumb
(g)	Rotary sensor	O	NA	O	Finger

Table III.1 Summary of previous development system

In this thesis, we designed portable and accurate a finger measurement system applying serially connected prismatic joint mechanism at the MCP joint unlike Fig. III.8 (g). The system has three rotary hall sensors and micro-controller board. And the sensors can measure the MCP, PIP and DIP joints respectively. The system was connected to an external power source and a communication cable with the laptop during the measurement, and then absolute each angle was transmitted to the laptop.

The serially connected prismatic joint mechanism consists of two prismatic joints and one rotational joint, and we can assume a human MCP joint as a rotational joint without A/A motion. Hence, the mechanism with MCP joint should be four-bar structure as shown in Fig. III.10. Fig. III.10 (b) and (c) show initial (extended) posture and last (flexed) posture, respectively. Two prismatic joints slide making the same stroke when a user flexes his/her finger, and then the revolute joint rotates the same angle as the user's MCP joint angle rotates as shown in Fig. III.10 (c).

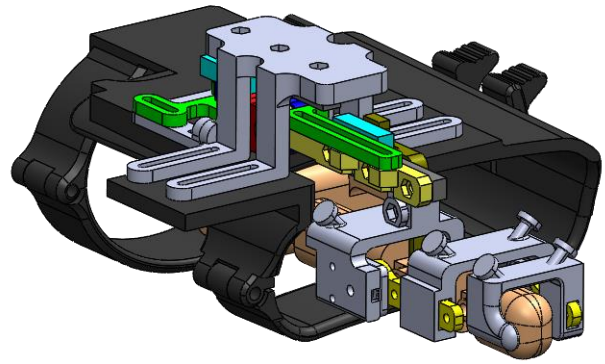

(a) Isometric View

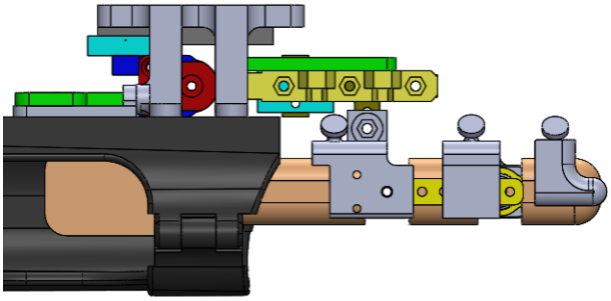

(b) Extension

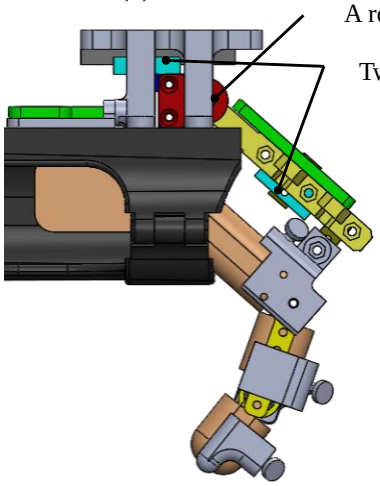

(c) Flexion

Fig. III.10 Principle of double prismatic MCP angle measurement system

The stroke is crucial to implement this mechanism to the system. Because the system should be on the hand, the stroke should be smaller than users' PP. The stroke of this mechanism was analyzed as shown in Fig. III.11. Two vectors, $\overrightarrow{OA}$ and $\overrightarrow{AB}$, are normal vectors each other. Hence the stroke can be calculated by (III.17). The stroke is proportional to *L1* which is the height of the structure and MCP joint angle. The initial stroke should be shorter than PP, therefore, the short height of the structure is

needed for one who has short fingers. The limitation of the developed system is that the available users are adult, not children.

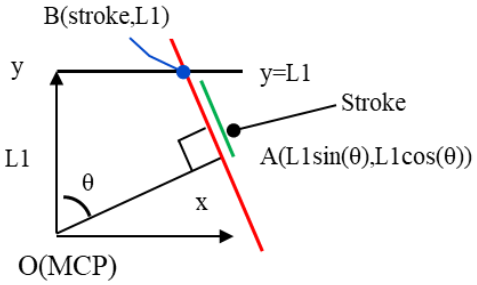

Fig. III.11 Stroke analysis at double prismatic structure

$$\frac{\cos\theta}{\sin\theta}\cdot\frac{\mathrm{L1}\cos\theta-L1}{\mathrm{L1}\sin\theta-stroke}=-1$$

$$\rightarrow \mathrm{L1}\cos^2\theta-L1\cos\theta+L1\sin^2\theta=\sin\theta\cdot stroke \qquad \text{(III.17)}$$

$$\rightarrow stroke=\frac{L1\left(1-\cos\left(\theta\right)\right)}{\sin\left(\theta\right)}=L1\cdot\tan(\frac{\theta}{2})$$

The other hall sensors coupled with PIP and DIP joints directly, and then measure the angles simultaneously.

To verify the developed measurement system performance itself, the experiment with an artificial hand was conducted before applying the real hand. The artificial hand was made as shown in Fig. III.10. The artificial joint angles were captured by both the developed system and the infrared camera-based motion capture system (Prime 13, Optitrack [24]). Total six markers were used: three for making coordinate vectors and the others for making phalanx vectors as shown in Fig. III.12. The experiment procedure was as follows;

1) connect the artificial hand to the developed system
2) attach the markers at each joint and fingertip
3) flex and extend the artificial finger naturally three times
4) repeat 1) to 3) eight times

Table III.2 showed the experimental result, the RMSE between the system and motion capture. The average RMSE joint angles were about 1˚ and the maximum joint angles errors were about 3˚. The only one result in the eight trials is shown to clearly explain the result and error as an example as shown in Fig. III.13. The developed system was followed well in Fig. III.13.

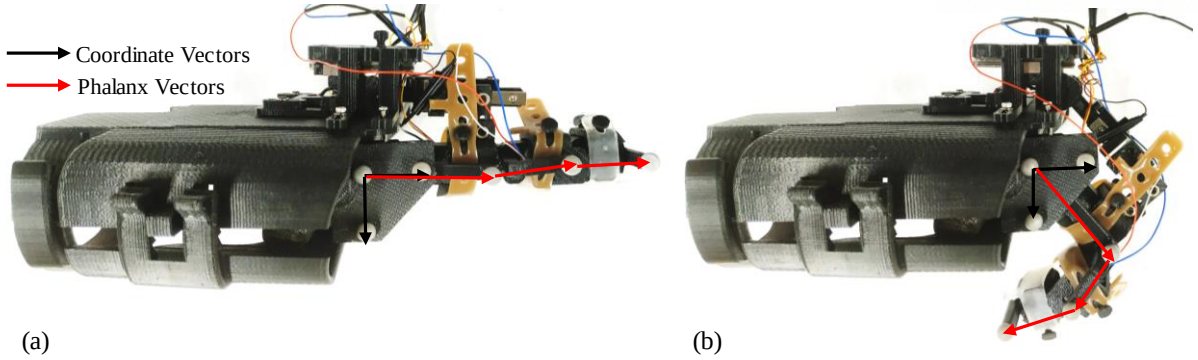

Fig. III.12 Experiment setup (artificial hand)

(a) Extension posture (b) Flexion posture. The black arrows are for the coordinates and red arrows are for the phalanx vectors.

Trial	Error	MCP	PIP	DIP
1	RMSE (˚)	0.96	0.68	1.32
	Max. Error (˚)	3.50	2.43	3.25
2	RMSE (˚)	1.47	0.92	1.28
	Max. Error (˚)	3.52	2.35	3.23
3	RMSE (˚)	1.85	1.48	1.66
	Max. Error (˚)	4.45	3.85	3.92
4	RMSE (˚)	0.88	1.01	1.53
	Max. Error (˚)	3.43	2.83	3.64
5	RMSE (˚)	1.21	0.98	1.84
	Max. Error (˚)	3.55	2.98	3.73
6	RMSE (˚)	1.55	1.25	1.65
	Max. Error (˚)	3.83	3.27	3.48
7	RMSE (˚)	1.99	1.58	1.26
	Max. Error (˚)	6.34	3.59	3.34
8	RMSE (˚)	1.30	1.71	2.10
	Max. Error (˚)	4.79	3.29	4.45
Average RMSE (˚)		1.40	1.20	1.58
Average Max. Error (˚)		4.17	3.07	3.63

Table III.2 Experiment result (artificial hand)

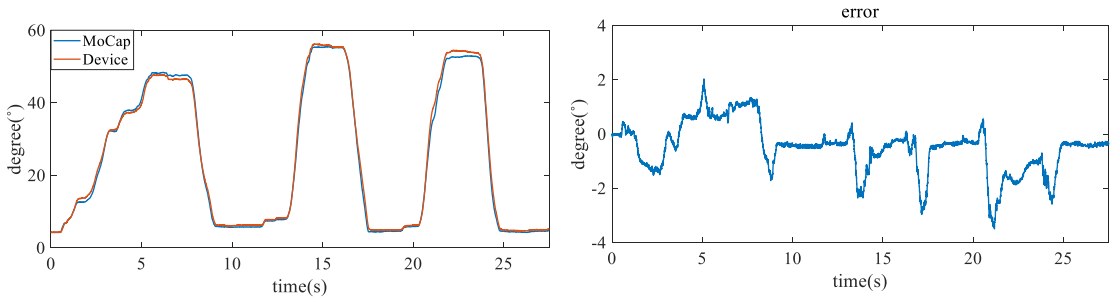

(a) MCP joint experiment result

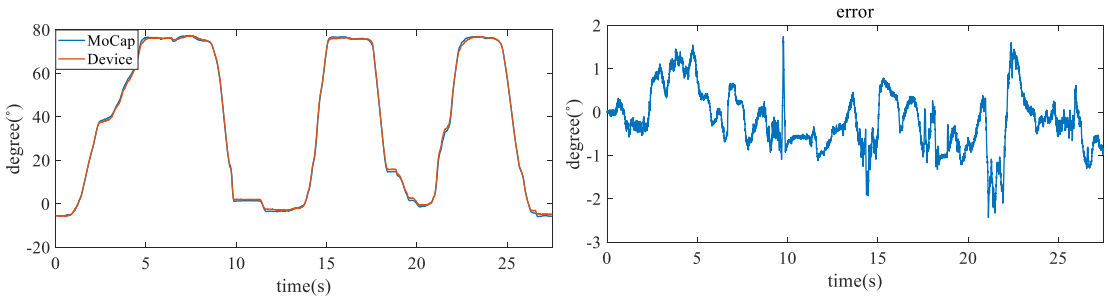

(b) PIP joint experiment result

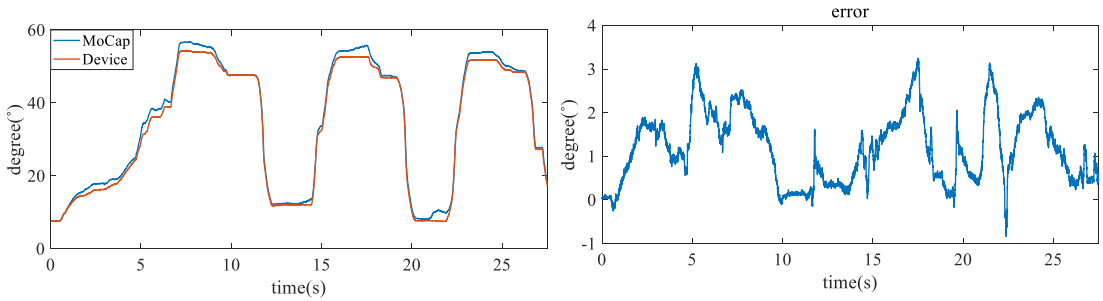

(c) DIP joint experiment result

Fig. III.13 Experiment result (artificial hand)

Each left figure shows results of two systems (motion-capture and developed system) and each right figure shows the error between the two systems

The finger motion measuring experiment was conducted to verify the developed finger motion measurement system performance with the real hand. The finger joint angles were captured by both our system and the infrared camera-based motion capture system (Prime 13, Optitrack [24]), and the joint angles from the two systems were compared. Total six markers were used: three for making coordinate vectors and the others for making phalanx vectors as shown in Fig. III.14. The experiment procedure was as follows;

1) Don our developed system.

2) Attach the markers at each joint and fingertip

3) Flex and extend the finger naturally three times

4) Repeat 1) to 3) four times

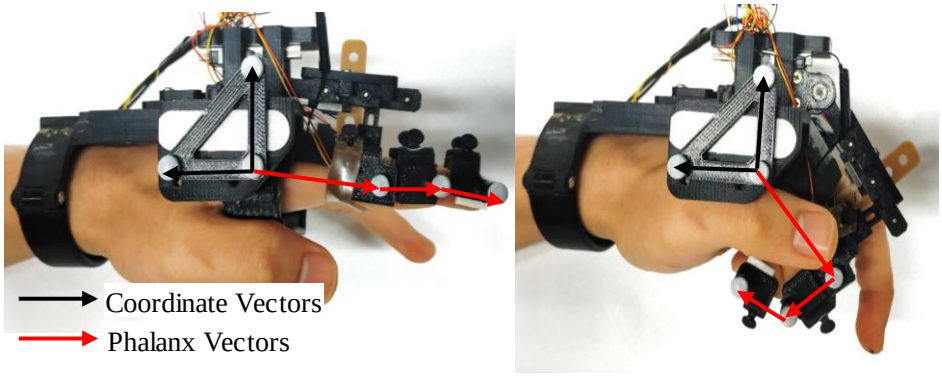

(a) (b)

Fig. III.14 Experimental Setup (real hand)

(a) Extension posture (b) Flexion posture. The black arrows are for the coordinates and red arrows are for the phalanx vectors.

Table III.3 showed the experimental result, the RMSE between the system and motion capture. The average RMSE joint angles were about 2˚ and the accuracy of our system was reliable than the previous system. The maximum joint angle errors were about 6˚. The only one result in the eight trials is shown to clearly explain the result and error as an example as shown in Fig. III.15. The developed system was followed well in the Fig. III.15. The main reason was that the wearable interface might wobble during the experiment. This is because when the subject flexed his finger, flesh and muscles of hand made the wearable interface unstable.

Trial	Error	MCP	PIP	DIP
1	RMSE (˚)	1.74	1.7	2.7
	Max. Error (˚)	5.16	6.1	8.3
2	RMSE (˚)	2.82	2.1	2
	Max. Error (˚)	6.77	5.6	5.4
3	RMSE (˚)	2.73	2	2.2
	Max. Error (˚)	7.05	5.1	6.8
4	RMSE (˚)	2.14	1.8	2.9
	Max. Error (˚)	6.03	4.8	9.7
Average RMSE (˚)		2.42	2.4	2.4
Average Max. Error (˚)		6.33	5.58	6.87

Table III.3 Experiment result (real hand)

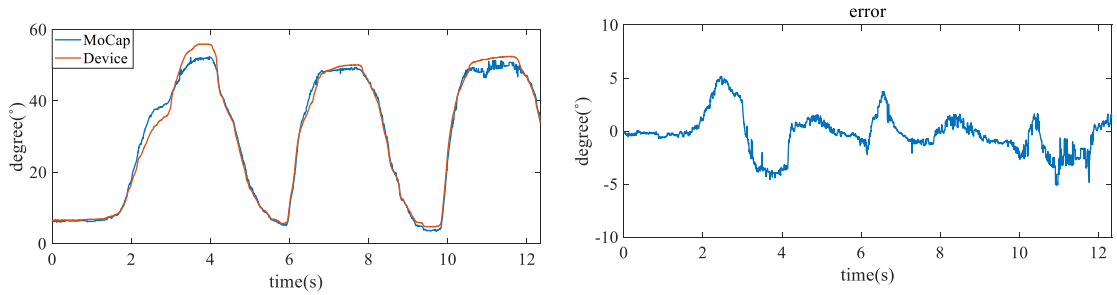

(a) MCP joint experiment result

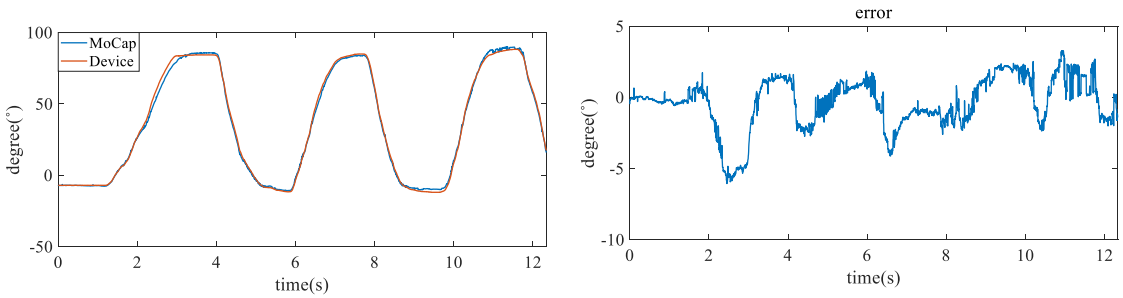

(b) PIP joint experiment result

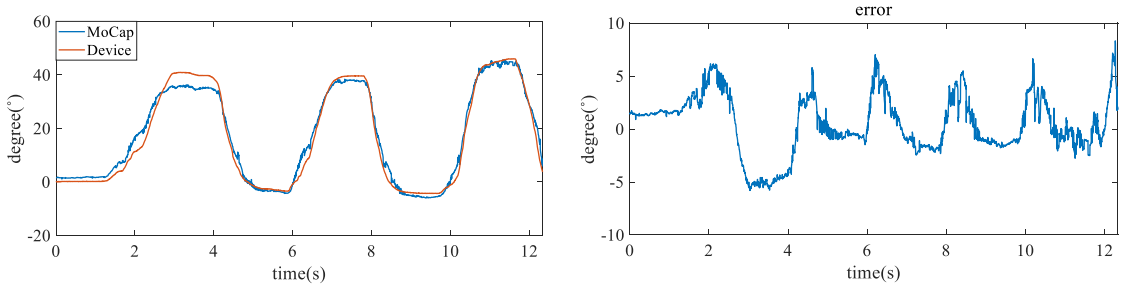

(c) DIP joint experiment result

Fig. III.15 Experiment result (real hand)

Each left figure shows result of two systems (motion-capture and developed system) and each right figure shows the error between the two systems

III.1.4.2 Finger Trajectory Analysis

As the proposed device is developed as the under-actuation system, we consider the parameters that can represent most general and consistent characteristics of the one DOF natural finger motion. The parameters can be a workspace of the finger, joint angle relationships between finger joints, a fingertip trajectory, etc. The workspace can be the parameter of the natural finger motion, however, itself means the range not the relations, so that generalized relation for designing the natural finger motion cannot be obtained. Other parameter, the joint angle relationship between the MCP and PIP joint, has a large variance in individuals as shown in Fig. III.16 (a). However, the fingertip trajectory is more consistent for each individual and can be expressed one DOF grasping motion as shown in Fig. III.16 (b) [25]. By considering many parameters of the finger motion, the fingertip trajectory can be the most general and consistent parameter to represent the natural finger motion.

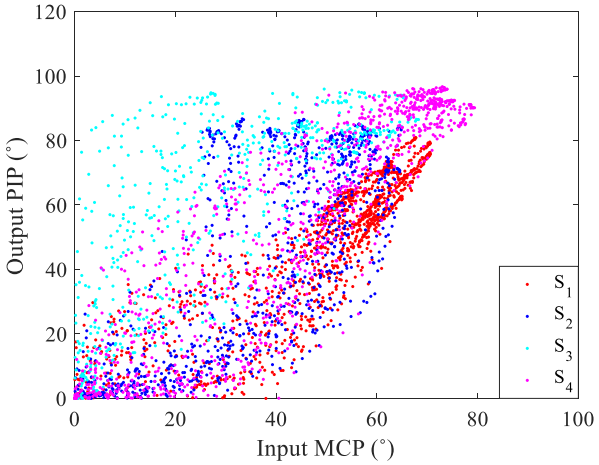

(a) MCP and PIP relationship

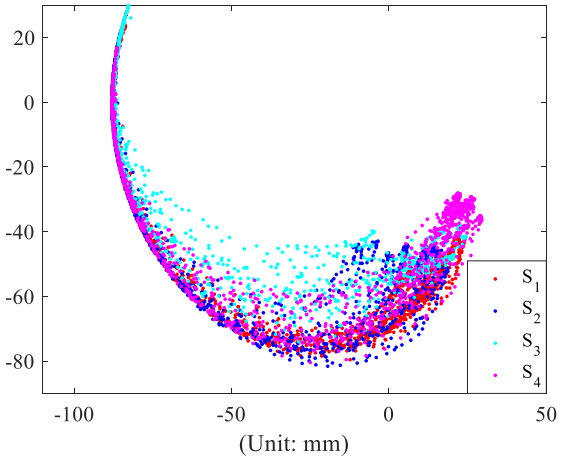

(b) Fingertip trajectories

Fig. III.16 Joint angle relationships and fingertip trajectories (four subjects)

To utilize the fingertip trajectory data of the amputee, the measured fingertip trajectory should be modeled as a relation to represent the measured data. Among many methods to model the fingertip trajectory, the representative is the logarithmic spiral curve [25, 26]:

$$r = ae^{\theta \cot \beta} \tag{III.18}$$

where a = 1.3394(finger length) – 23.255, β = 1.66±0.05 radians [26]. However, this equation does not cover the fingertip trajectory around the maximum flexion state because they just modeled the fingertip trajectory in the situation when the subject grasped and released specific objects. It means that the finger does not reach the maximum flexion state during that finger motion.

In this thesis, a new curve fitting method is proposed, which can express fingertip trajectory even at the maximum flexion state. The proposed observations are that the finger motion can be expressed as a series of rotation motions of three phalanges and the rotation motions can be easily expressed in polar coordinate. Thus, the finger motion can be expressed in the polynomial form of r and θ. The polynomial equation in terms of r and θ can be derived as follows.

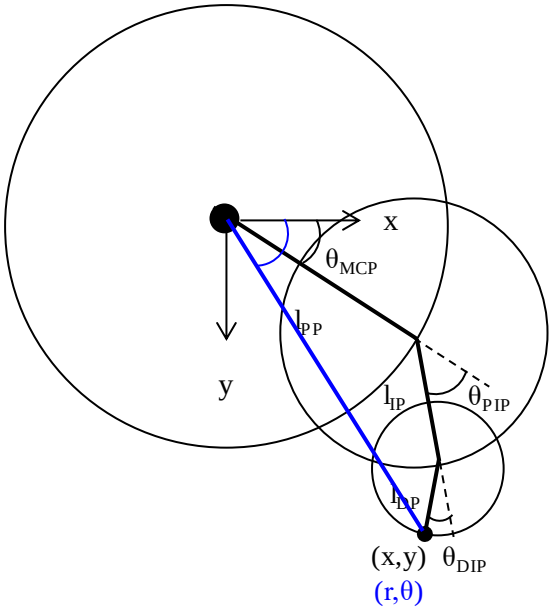

Fig. III.17 Link and angle parameters for kinematic analysis

(l_{PP}, l_{IP} and l_{DP} are length of PP, IP and DP, and θ_{MCP}, θ_{PIP} and θ_{DIP} are the MCP, PIP and DIP joint angles, respectively.)

The fingertip position in Cartesian coordinate can be expressed as:

$$\begin{aligned} x &= l_{PP}\cos(\theta_{MCP}) + l_{IP}\cos(\theta_{MCP}+\theta_{PIP}) + l_{DP}\cos(\theta_{MCP}+\theta_{PIP}+\theta_{DIP}) \\ y &= l_{PP}\sin(\theta_{MCP}) + l_{IP}\sin(\theta_{MCP}+\theta_{PIP}) + l_{DP}\sin(\theta_{MCP}+\theta_{PIP}+\theta_{DIP}) \end{aligned} \tag{III.19}$$

The fingertip position in Cartesian coordinate can be expressed as:

$$x^2 = \alpha + \beta + \gamma + \delta + \varepsilon + \varsigma$$
$$y^2 = -\alpha + \beta - \gamma + \delta - \varepsilon + \varsigma \quad \text{(III.20)}$$

where $\alpha = \frac{l_{DP}^2 \cos(2\theta_{DIP} + 2\theta_{MCP} + 2\theta_{PIP})}{2} + \frac{l_{PP}^2 \cos(2\theta_{MCP})}{2} + \frac{l_{IP}^2 \cos(2\theta_{MCP} + 2\theta_{PIP})}{2}$,

$\beta = \frac{l_{DP}^2}{2} + \frac{l_{IP}^2}{2} + \frac{l_{PP}^2}{2}$, $\gamma = l_{IP} l_{PP} \cos(2\theta_{MCP} + \theta_{PIP}) + l_{DP} l_{PP} \cos(\theta_{DIP} + 2\theta_{MCP} + \theta_{PIP})$,

$\delta = l_{DP} l_{PP} \cos(\theta_{DIP} + \theta_{PIP})$, $\varepsilon = l_{DP} l_{IP} \cos(\theta_{DIP} + 2\theta_{MCP} + 2\theta_{PIP})$, and

$\varsigma = l_{DP} l_{IP} \cos(\theta_{DIP}) + l_{IP} l_{PP} \cos(\theta_{PIP})$.

The distance (r) from the MCP joint to the fingertip can be written using (III.19) as:

$$r = \sqrt{x^2 + y^2}$$
$$\rightarrow r = \sqrt{2(\beta + \delta + \varsigma)}$$
$$\rightarrow r = \sqrt{l_{DP}^2 + 2\cos(\theta_{DIP}) l_{DP} l_{IP} + 2\cos(\theta_{DIP} + \theta_{PIP}) l_{DP} l_{PP} + l_{IP}^2 + 2\cos(\theta_{PIP}) l_{IP} l_{PP} + l_{PP}^2} \quad \text{(III.21)}$$

Under the assumption that the proportion of each finger phalanx (l_{PP}:l_{IP}:l_{DP}) is 5:3:2 [27], and PIP and DIP joint angles have 1:0.76 ratio [28], (III.21) can be rewritten as

$$r = \frac{\sqrt{2}\sqrt{l^2\left(6\cos\left(\frac{19\theta_{PIP}}{25}\right) + 10\cos\left(\frac{44\theta_{PIP}}{25}\right) + 15\cos(\theta_{PIP}) + 19\right)}}{10} \quad \text{(III.22)}$$

By considering that the ROM of the PIP joint is 0~105º [16], cosine terms can be rewritten as forth order of the Taylor expansion as:

$$r \approx \frac{\sqrt{2} l \sqrt{\left(4.7\theta^4_{PIP} - 24.72\theta^2_{PIP} + 50\right)}}{10} \quad \text{(III.23)}$$

Finally, (III.23) can be expressed as the second order polynomial form:

$$r = a\theta^2 + b\theta + c \quad \text{(III.24)}$$

The Fig. III.18 shows the measured finger trajectory of the subject and the results of two curve fitting method: logarithmic spiral curve and the proposed method. Black dots are the measured data, blue line is the fitted curve of logarithmic spiral curve, and red line is proposed curve of the second polynomial by the polar coordinate analysis. The root mean square errors (RMSE) are 4.6 and 1.7 mm, respectively. The logarithmic spiral curve does not match to the measured fingertip trajectory as the finger flexes, on the other hand, the proposed curve shows better fitting performance even at the maximum finger flexion.

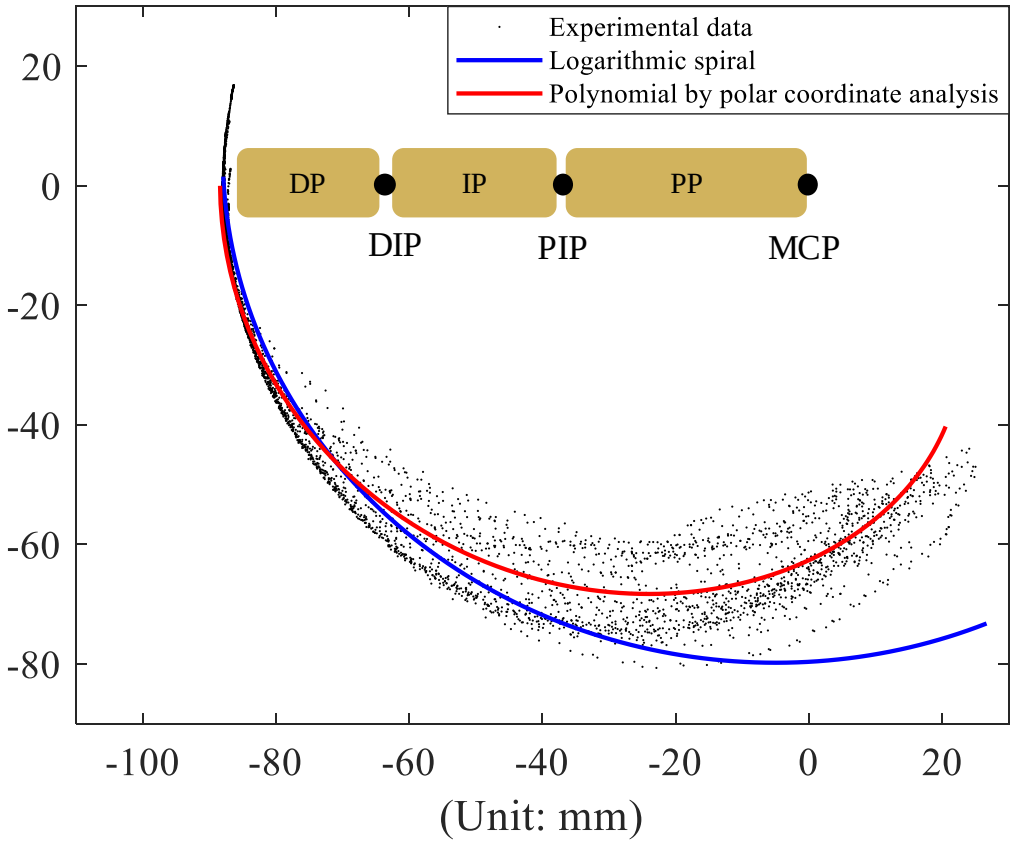

Fig. III.18 Comparison between logarithmic spiral curve and proposed method

III.1.5 Design Optimization

The considerations of the appropriate four-bar mechanisms and the desired fingertip trajectory analysis for the natural finger motion were explained so far. In this section, the optimization method of each link length is discussed to satisfy the requirements of the practical finger prosthesis and to customize the device for each amputee by following goals; 1) the size of the prosthesis should not be larger than the patient's finger size, and 2) the prosthesis should move as the natural finger motion of the amputee.

The variables as shown in Fig. III.19 are used at the cost function of optimization algorithm. The positions of the D, G, and H joints are fixed to match the finger joint of the system with the amputee's actual finger joint (i.e., l_{PP}, l_{IP}, l_{DP} etc. in the gray boxes are fixed variables). The other variables are the design variables to minimize the following cost function:

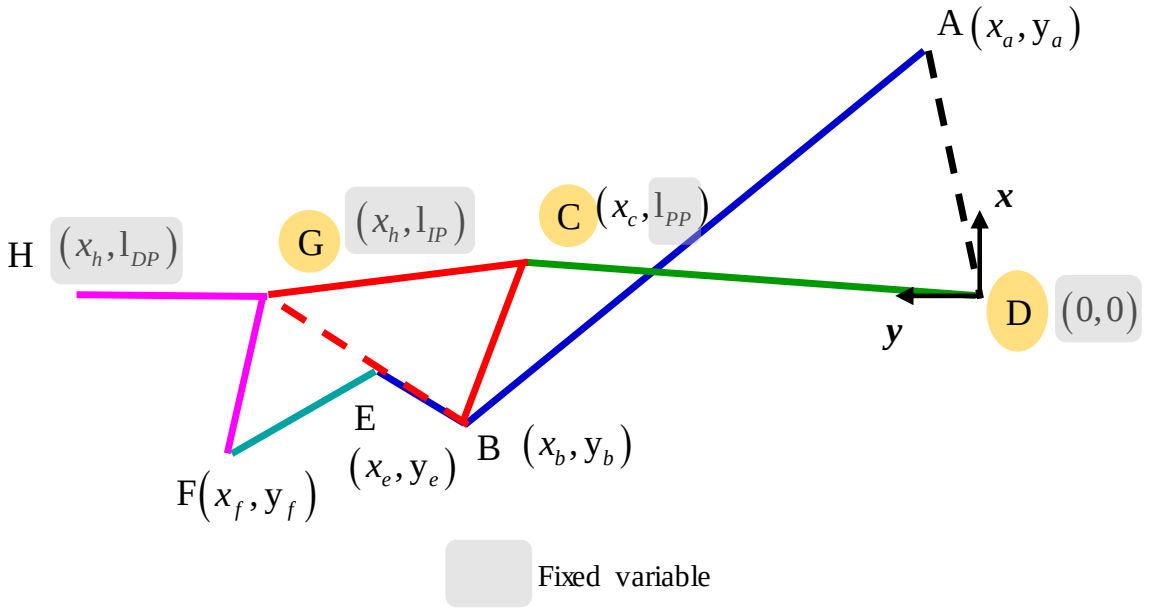

Fig. III.19 Variable analysis for the optimization

$$x_i = \left[x_a \; y_a \; x_b \; y_b \; x_c \; x_e \; y_e \; x_f \; y_f \right] \tag{III.25}$$

where subscripts of x and y means the positions of each joint in the direction of *x*-, *y*- axis as shown in Fig. III.19.

The cost function is as follows:

$$J = w_1\sqrt{(\hat{\vec{y}} - \vec{y})^2} + w_2\sqrt{(\theta_{MCP}^{R.\max} - \theta_{MCP}^{MAX})^2} + w_3\sqrt{(\theta_{PIP}^{MAX} - 1.1\theta_{MCP}^{MAX})^2} + w_4\sqrt{(\vec{\theta}_{DIP} - 0.76\vec{\theta}_{PIP})^2} \tag{III.26}$$

where w_i are weight factors, $\hat{\vec{y}}$ is reference finger trajectory vector, $\vec{y}$ is prosthesis trajectory vector, $\theta_{MCP}^{R.\max}$ is the reference maximum MCP joint angle, θ_{MCP}^{MAX} and θ_{PIP}^{MAX} is the maximum MCP and PIP joint angle of prosthesis, respectively, and $\vec{\theta}_{PIP}$ and $\vec{\theta}_{DIP}$ are PIP and DIP angle vectors of the prosthesis.

The first term is to minimize the error between the fingertip trajectory of the prosthesis ($\hat{\vec{y}}$) and the measured fingertip trajectory of the patient ($\vec{y}$). The other terms are not only to follow the fingertip trajectory but also to make more natural finger motion by considering finger joint relationships and ROM of the finger joints. Second and third terms are added to satisfy ROM of each joint in our prosthesis by considering the practical issues. Practically, most amputees have experienced the swelling phenomenon, an abnormal enlargement of the amputated part. The proposed system should consider the collision to the swollen part which can reduce ROM of the system. Therefore, not normal ROM but function ROM explained in section 2.1 is considered to design the optimization criteria. The second term is for the system to minimize difference between amputee's functional ROM of the MCP joint (i.e.,

the maximum MCP joint angle) and the ROM of the system. The third term is used for the maximum PIP joint angle to be similar to 1.1 times MCP maximum joint angle [2]. In general, the MCP and PIP joint angle relationship may not be generalized for each person, however, the maximum of two joint angles (the MCP and PIP joints) are known to have consistent relationship [16, 29, 30]. The last term shows the PIP and DIP joint angle relationship where the joint angles have 1:0.76 relationship [28]. w_i are weighting factors and manually tuned for each term so as to have similar gradient.

The optimization process is illustrated in Fig. III.20. First, the range of fixed point and design variables which locate joints of the prosthesis within the finger size is chosen. To decrease computation time, the subrange of design variables is manually determined, and the cost function values are calculated using the design variables in that subrange. If the collisions occur between links and/or the residuum, those design variables will be excluded from the candidate of optimization results. If optimized design variables in the subrange are in the lower or upper bounds, the subrange of the design variables will be modified, and the optimization process will be repeated in the modified subrange. If the optimized design variables are not located in any lower and upper bound values, finally, the design variables will be chosen as optimization result and the optimized link lengths will be calculated.

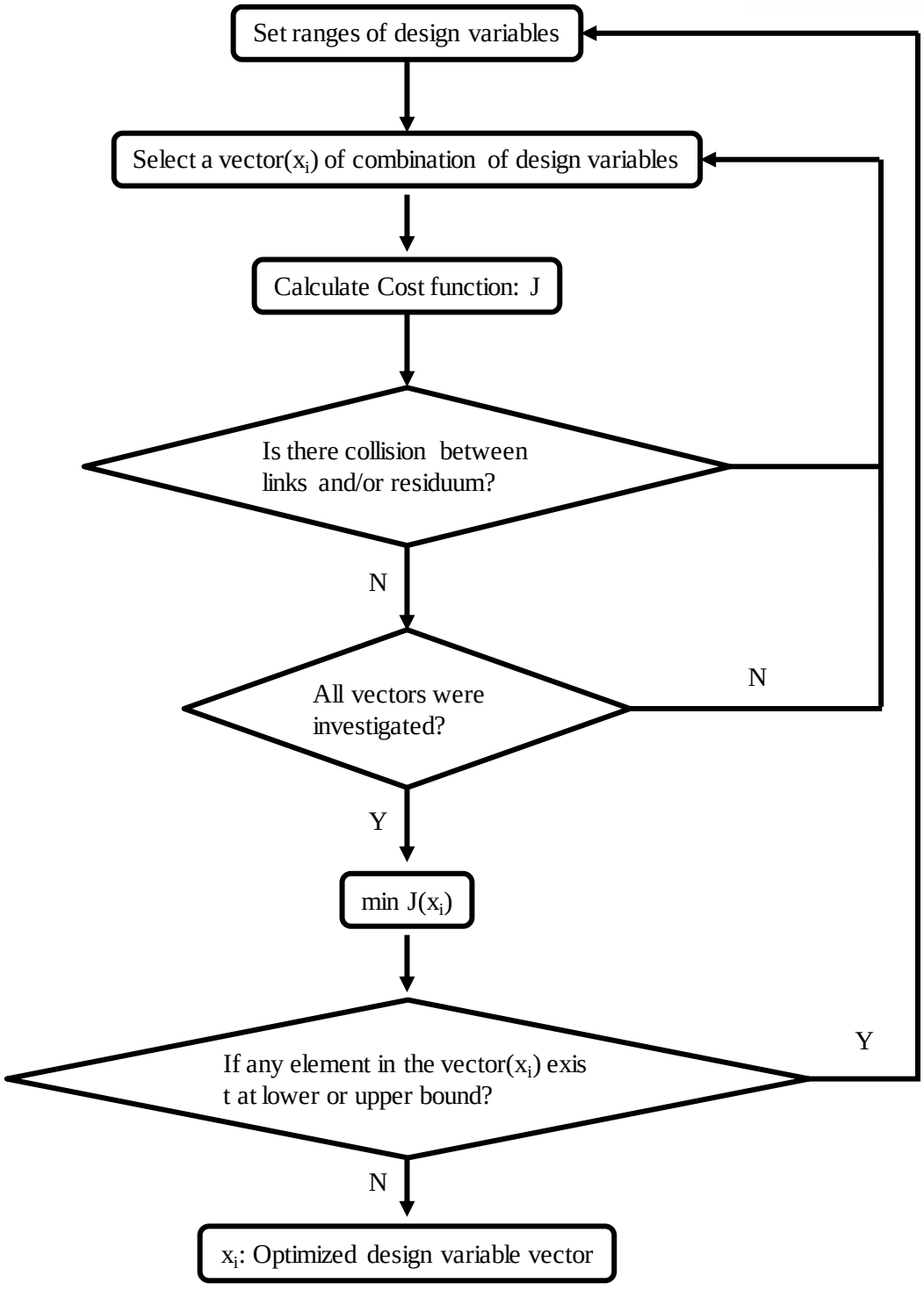

Fig. III.20 Optimization algorithm

III.1.6 Modular Wearable Interface

In this thesis, the modular wearable interface which allows the user to easily wear and fix the system is proposed as shown in Fig. III.21. For the ideal finger prosthesis, wearing method should be easy and the alignment of the finger joints and the system joints should be accurate. Previously developed systems are usually made as integrated systems which combine the covering part (the dorsum of the hand) and the fixing part (the finger) so that, if the joints of the system and the finger are not suitably matched, the user has to doff and re-don whole system to fit well [31].

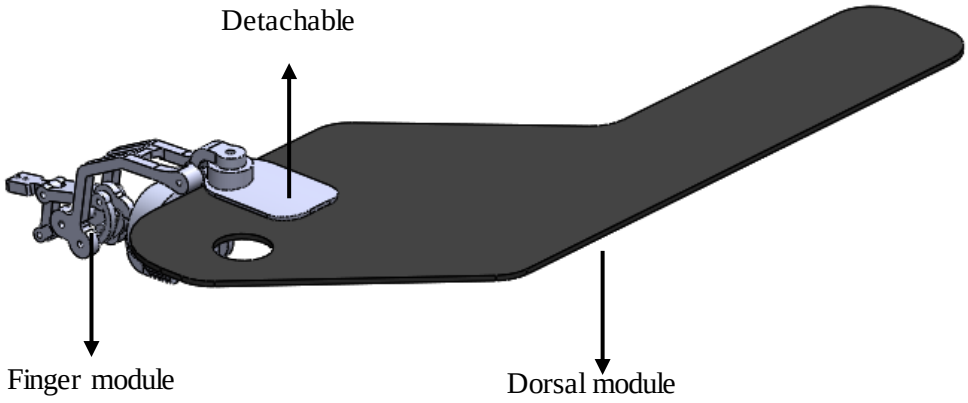

(a) Modular wearable interface

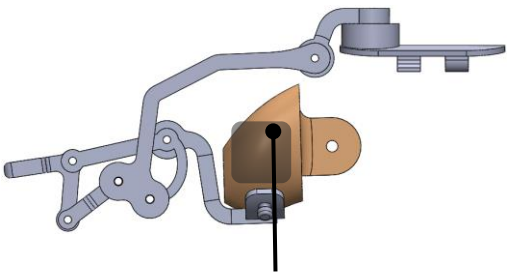

(b) Wearable method of the finger module (c) Wearing the overall system

Fig. III.21 Modular wearable interface

(a) modular wearable interface; the finger and dorsal modules can detachable/attachable using the Velcro, (b) wearing method of the finger module; the finger module can be fixed at the residuum using urethane band, (c) Overall wearable interface

On the other hand, the proposed modular interface prevents the user from whole taking off and re-don process by dividing dorsal and finger wearable interfaces; the user putted on each module, dorsal and finger, separately, and the each module is combined by Velcro as shown in Fig. III.21 (a). The user

could don the prosthesis fit well. By the modular wearable interface, the user can wear the system properly by manually adjusting the system joint to match the finger joint.

Moreover, the proposed wearable interface has other advantages than the previously developed systems. Many previous systems have used the stationary ground, which is the start point of actuation where the structure does not move, near the wrist, resulting that free wrist motion is disturbed [9, 10]. The proposed dorsal module does not interfere with free wrist motion, because its material is soft fabric and it is fixed by covering whole back of the hand not near the wrist. The finger module can be designed according to the amputee's swelling residuum. The connecting part between the residuum and the module can be designed by considering the contour of swelling residuum and, therefore, can fit well to the swelling residuum. The finger module and wearing the whole system are shown in Fig. III.21 (b) and (c), respectively.

III.1.6.1 Fixing point for the Dorsal module

Three types of fixing methods for the dorsal module are considered as shown in Fig. 22: (a) the finger and wrist points fixing, (b) the finger, dorsal/palm and wrist points fixing and (c) the finger and dorsal/palm fixing. First, the finger and wrist fixing method can grasp stable, however, it cannot be stable during extension motion as shown in Fig. 22 (a). The wrist should be moved back to hold the especially thick object. Second, the finger, dorsal/palm, and wrist points fixing method grasp always stable, however, it can make the user uncomfortable due to the three fixing points as shown in Fig. 22 (b). Finally, the proposed method, the finger and dorsal/palm fixing method, have similar grasp performance to the method (b), and it also makes the user uncomfortable because the palm is pressed. To solve this problem, we proposed an open palm design using soft materials.

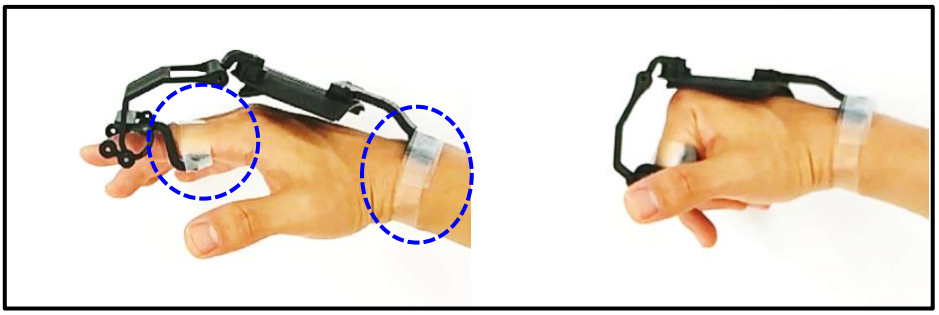

(a) Two points fixing: the finger and wrist

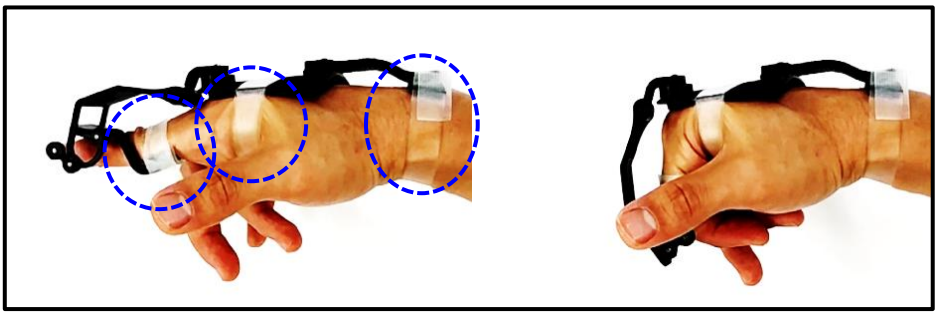

(b) Three points fixing: the finger, dorsal/palm and wrist

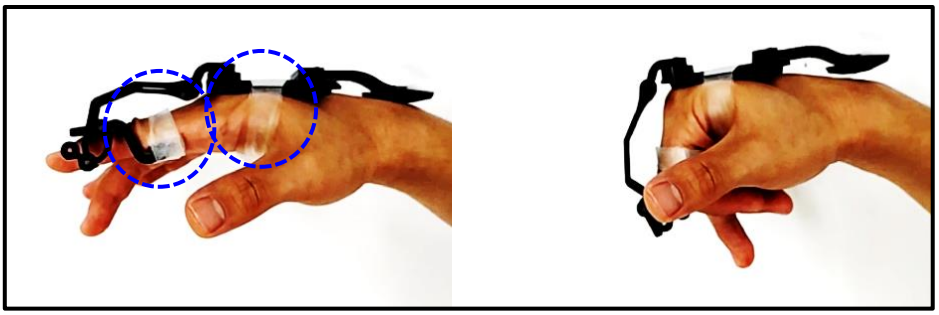

(c) Two points fixing: the finger and dorsal/palm (proposed method)

Fig. 22 Three types fixing methods for the dorsal module

III.1.6.2 Fabrication of the two Dorsal modules

In this thesis, two methods are used to make the soft dorsal module: silicone mold and tailoring fabric methods. First, the silicone mold method can have a better fit to the dorsum of the subject and similar color of the subject's skin by adding the pigment. The fabrication method of the silicone dorsal module is as follows;

1) design the mold considering the shape of the dorsum of the subject as shown in Fig. III.23 (a).

2) mix the part A and part B of the silicone material, (and the pigment).

3) degas the silicone material to eliminate any entrapped air in the vacuum chamber for about two minutes.

4) pour the degassed silicone onto the mold as shown in Fig. III.23 (b).

5) cure the mold at the room temperature for 24 hours.

6) demold the dorsal module shown in Fig. III.23 (c).

The fabricated silicone dorsal module is shown in Fig. III.23 (d). The incarnadine color was used for the aesthetic side in process 2).

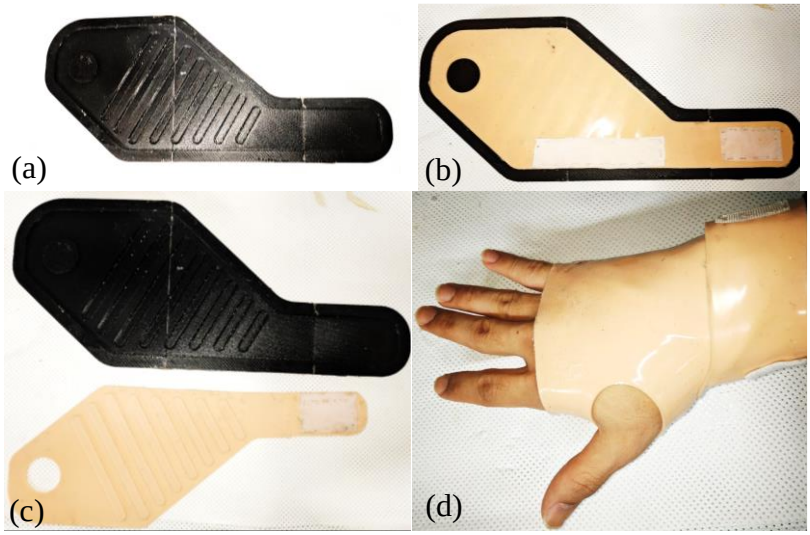

Fig. III.23 Silicone mold dorsal module fabrication method

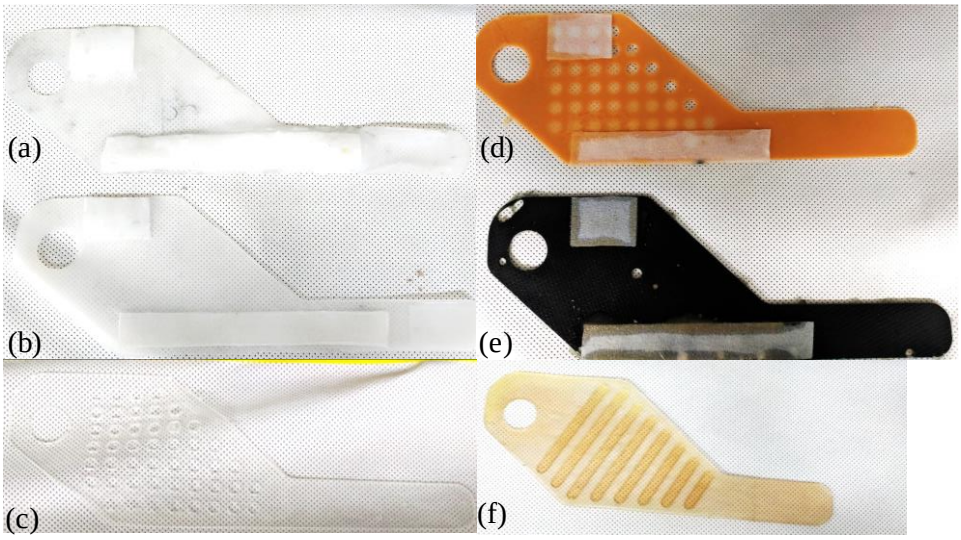

Fig. III.24 Various samples from the first method

(a) Eco flex 00 30 (b) Dragon skin 30A (c) Clear Flex 50A with various hexagon holes (d) PMC-780 80A with various hexagon holes and incarnadine color (e) PMC-780 80A with embossing surface finishing and black color (f) Clear Flex 90A with the teeth of a comb shape

The various materials and mold designs were tried using the first method to fit well as shown in Fig. III.24. First, to find the proper strength of the material, five materials which have the different modulus from 00 30 to 90A shore hardness was chosen. The Eco flex 00 30 and Dragon skin 30A in Fig. III.24

(a) and (b), respectively, was too soft to fix the module. And the Clear Flex 50A and Clear Flex 90A in Fig. III.24 (c) and (f), respectively, had the bad wearable feeling which was too sticky. Among those materials, PMC-780 80A had the best fit and the proper strength.

Hence, this method could control the strength by changing the silicone materials which have the various modulus, and even had high hygiene by easily washing with water. However, the hand was sweated when the subject wore the silicone dorsal module, which may cause uncomfortable to the subject. To deal with this problem, various mold design were reviewed; the various hexagon were holed to ventilate the air maintain the strength as shown in Fig. III.24 (c) and (d), the embossing surface finishing was added to reduce the contact surface as shown in Fig. III.24 (e), and the teeth of a comb shape was added to ventilate the air in Fig. III.24 (f). Even though the various methods were reviewed to ventilate air, it was not effective. Therefore, the second method was considered.

The second method of the dorsal module is tailoring fabric. This fabric has three layered: the jersey for the inner, the neoprene with many small holes for the fitting and ventilation, and the loop for the Velcro. And this fabric can have different color by a requesting specific order to the manufacturer as shown in Fig. III.25 (c). The fabrication method is very simple; design the mold same as 1) in the first method process, and just tailor the fabric by the laser machine (C40, Coryart [32]). Three samples made by the second method is in Fig. III.25; (a) the layered neoprene fabric was tailored, (b) was tailored with various hexagon holes and (c) the skin color fabric was tailored. The hexagon holes made the wearable module have low strength so that it was not proper in Fig. III.25 (b).

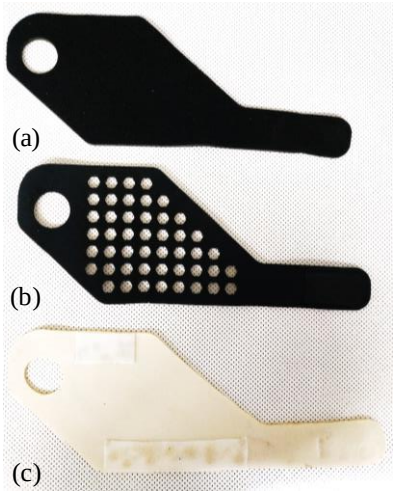

Fig. III.25 Three samples from the second method

(a) basic tailoring, (b) tailoring with various hexagon holes and (c) basic tailoring with the colored fabric

III.2 Results and Discussion

The performance of the proposed system was verified with the undamaged subject before applying to the finger amputee. Since our system could not be worn on normal hand, the system was modified as shown in Fig. III.26. During the experiment, the index finger was maintained to the hyper-extended posture, the motion of the system was actuated by the MCP joint motion of the middle finger. The middle finger interface in Fig. III.26 connected the subject's middle finger and the finger module of the system. Although the system was worn in different ways from what we designed, the working mechanism of the modified system was same as our origin system, which could show similar results.

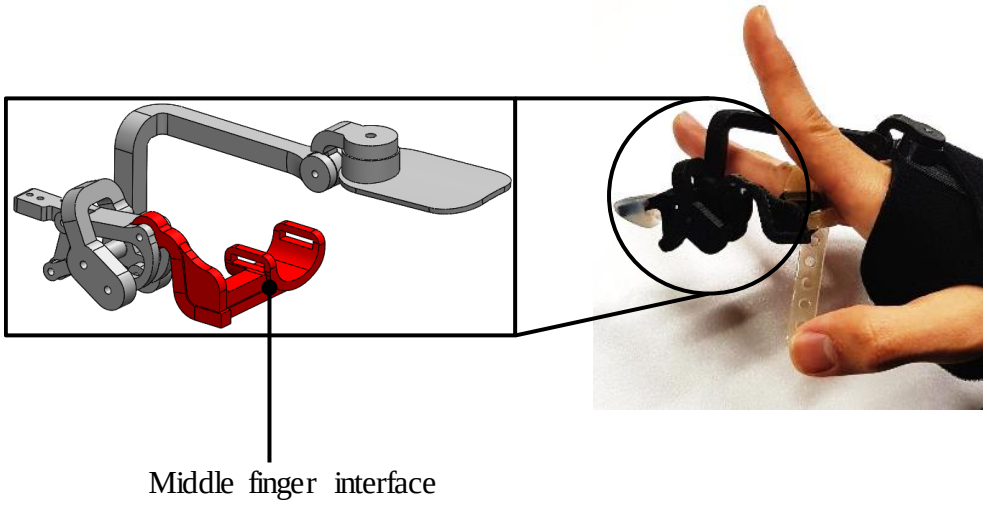

Fig. III.26 Modified finger module interface for the experiment

III.2.1 Optimized Design

The results of the optimization process are shown in Fig. III.27. In Fig. III.27 (a), the red line is desired fingertip trajectory fitted from the measured trajectory of the subject (black dot) and the blue line is the optimized trajectory of the proposed system. The reason of the difference in the two trajectories was that the design variables which made the collisions between the swollen residuum and the structure were excluded. The relationship between the PIP and DIP joint angles was described in Fig. III.27 (b). The black dots are experimental results of the subject and the red line is the desired slope of the DIP joint angles over the PIP joint angles. The desired slope was 0.76 in the cost function and the result was 0.77, which the optimization was completed to satisfy the desired relationship between the PIP and the DIP joint angles. Lastly, as mentioned in the previous section, the proposed system was optimized to satisfy the functional ROM (i.e. maximum joint angle) of the MCP and the PIP joints. The results of the optimization was that the MCP joint maximum angle was satisfied as the 75˚, but the PIP joint angle was 63˚, which was lower than the functional ROM of the PIP joint [16]. This is because the design variables which realized the functional ROM of the PIP joint caused the collisions between the swollen part and the structure. However, the RMSE between the trajectory of the subject and that of the

proposed system is small as 3 mm, which is similar to the fingertip resolution 2.5 mm [33].

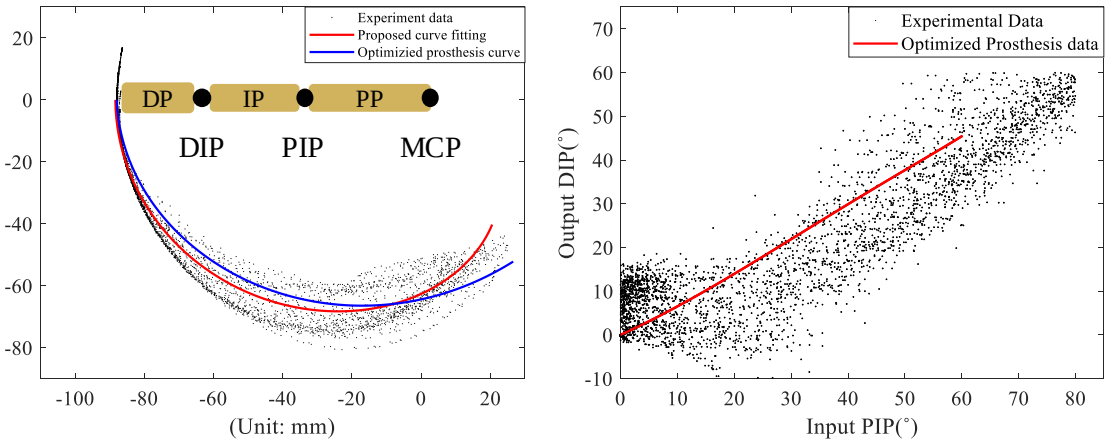

(a) Fingertip trajectory (b) Relationship between PIP and DIP joint

Fig. III.27 Optimization result

(a) the fingertip trajectory and (b) the PIP and DIP joint relationship

Through the proposed optimization process, the fingertip trajectory, the functional ROM and the relationship between joint angles were closely satisfied to the desired relations so that the natural finger motion of the subject was realized by the proposed system.

III.2.2 Fingertip Trajectory Generation

The performance of the fingertip trajectory generation was verified through an infrared camera-based motion capture system (Prime 13, Optitrack [24]). The experiment setup is shown in Fig. III.28. Total six markers were used in the experiment: three markers for the reference coordinate, two markers for measuring A/A motion of the finger and the last one for measuring fingertip position. The subject did F/E motion five times naturally in each trial and total six trials were accomplished.

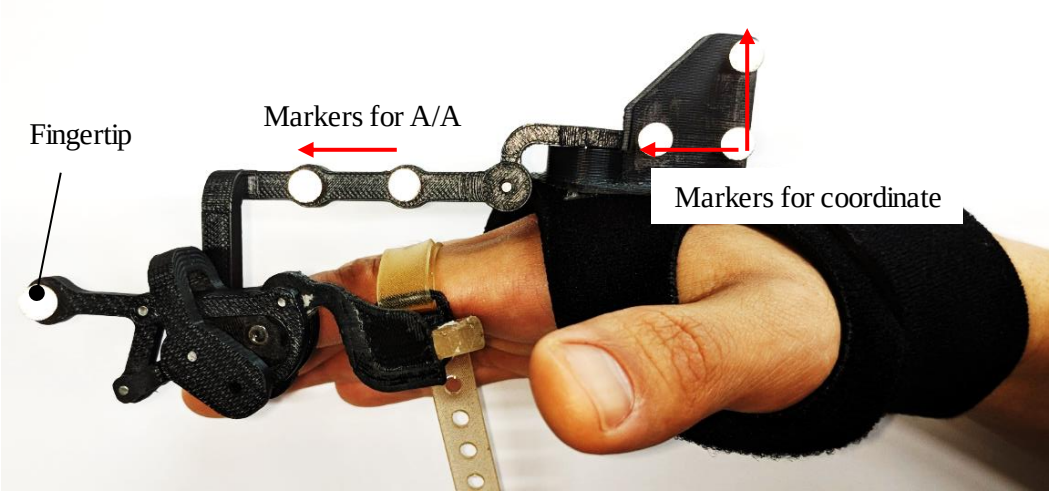

Fig. III.28 Experimental setup of fingertip trajectory generation

Fig. III.29 shows the result of fingertip trajectory generation. The only one result in the six trials is shown to clearly explain the result as an example. As the desired fingertip trajectory was expressed in the polar coordinate, the experimental result was also fitted in the polar coordinate to calculate the error of the trajectory generation. The average RMSE from six trials is 2.25 mm. The error may be arisen from the wavering of the wearable interface during the finger motion due to the movement of flesh and muscles of the dorsum of hand. However, the error of 2.25 mm is reasonable because it is smaller than the finger position sensing resolution [33].

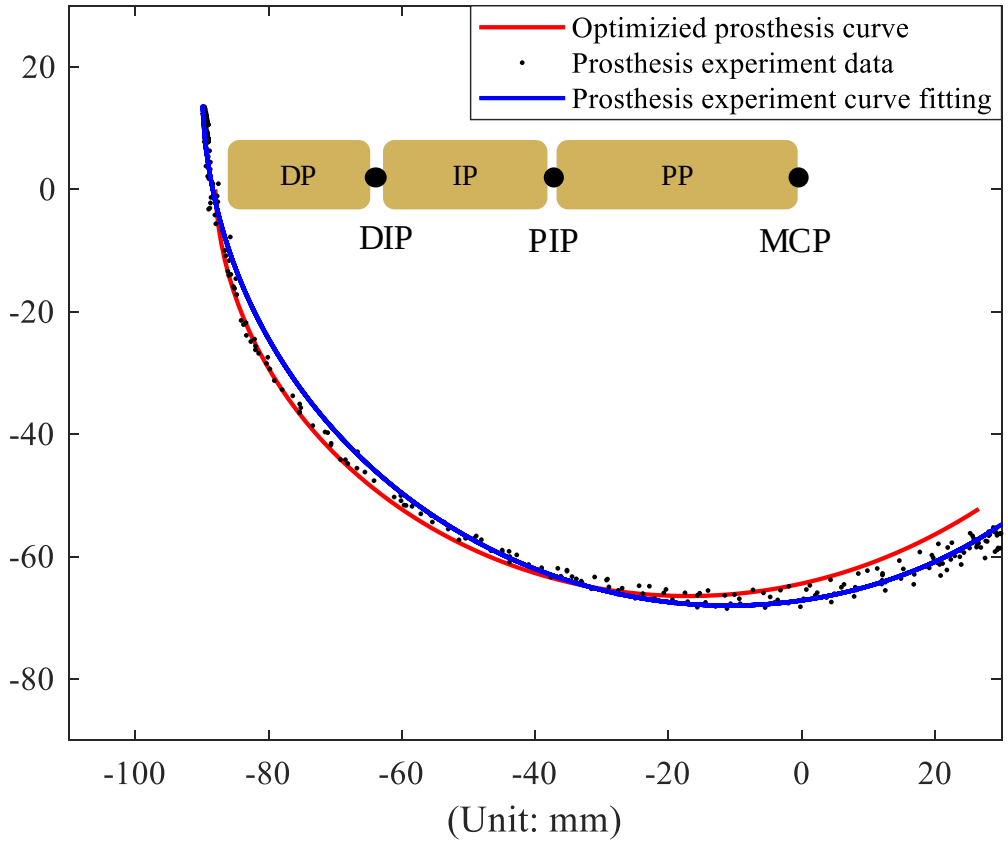

Fig. III.29 Fingertip trajectory experiment result.

III.2.3 Grasping Performance

Since the proposed system was designed to help grasping and manipulating objects, in this thesis, the experiment of the grasping performance was conducted. The targeted grasping tasks were chosen by considering whether the index finger was dominant because the proposed system was developed for the index finger amputee. T.feix et al classified the grasping tasks into 33 categories; tip and palmar pinch are the dominant grasping tasks which the index finger is mainly engaged in [34]. Therefore, the two grasping tasks of the tip and the palmar pinch were chosen for verifying the grasping performance of the proposed system. The difference between the palmar pinch and the tip pinch is that which part of

the finger is used for the grasping motion; the palmar pinch uses the most areas of the distal phalanx and tip pinch uses only the tip of the distal phalanx as shown in Fig. III.30 (a) and (b).

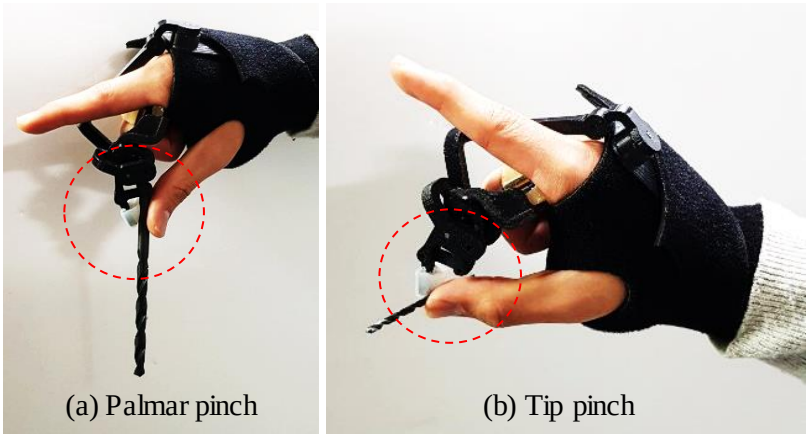

Fig. III.30 Two grasps used in the grasp experiments
(a) palmar pinch and (b) tip pinch

The experimental procedure was inspired from Southampton Hand Assessment Procedure (SHAP) which evaluate the performance of the upper limb prosthesis including the hand prostheses [35]. The SHAP consists of 20 tasks: 'six abstract object tasks' at which the people grasp and move six wooden object using different types of the grasping motion and '14 ADL tasks' at which the subject carries out various tasks such as glass jug pouring, jar lid, page turning and so on. Each completion time is measured during the tasks. In this thesis, we chose the tasks of grasping and carrying the objects in ‘six abstract object tasks’ and measuring the experimental time, and modified the experimental setup to evaluate the only grasping performance with and without the finger prosthesis. The modified experimental setup is shown in Fig. III.31. Before the experiment, the subject had enough training time to practice the usage of the proposed system and comprehend the experiment. After wearing our prosthesis, the subject grasped the cylinder object on the left side using palmar or tip pinch grasp, carried the object over the barrier in the middle of bench, put off the object on the hole or the pedestal of the right side, and the time was measured in each trial. If the subject had missed the object during grasp, the subject re-grasped the object as quickly as possible. The experimental time was measured from the start posture to the end posture. At the start posture, the subject gathered the hand in front of the chest and said “start” to the experimenter. After the grasping task, the subject gathered the hand again in front of the chest and said “end” to the experimenter. The experimental time was measured between the voice of “start” and “end”.

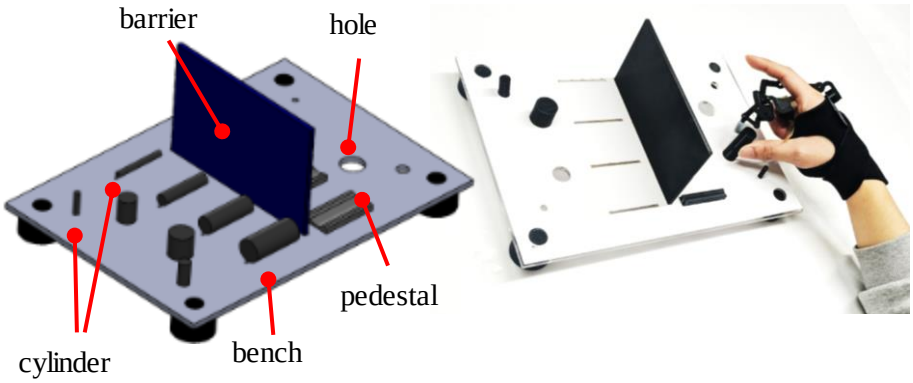

Fig. III.31 Grasping task bench

Four different diameter cylinder objects with 50mm length were used in the experiment: 5, 10, 15 and 20mm. The objects were placed vertically or horizontally so that the subject could naturally hold the object using palmar or tip pinch; the subject used the most area of the distal phalanx to grasp the vertically placed object as the palmar pinch and the tip of distal phalanx to grasp the horizontally placed object as the tip pinch. The detailed experiment procedure is as follow;

1) Grasp the object among the various diameter cylinder objects.
2) Carry the object over the barrier.
3) Put off the object on the hole or the pedestal, and the time is measured.
4) Take a break for 10 seconds.
5) Retry 1) to 4) until all objects are moved.
6) Repeat 5 times for each grasp (palmar and tip pinch).

The experiment results are shown in Table III.4. The result of one subject was shown in this thesis because the prototype was customized according to the subject's information such as the length of the finger phalanges, the fingertip trajectory and so on.

In Table III.4, there was only one failure of grasping in the total experiments of palmar and tip pinch (40 trials). The subject re-grasped the cylinder quickly and even accomplished the trial in one failure. It means that the grasping performance itself was successfully achieved with the proposed system.

In the case of the palmar pinch, it took average 3.45 seconds with normal hand and 3.92 seconds with our prosthesis. The differences between them were about 0.4 seconds, thus our prosthesis could have similar performance compared to the normal hand at the palmar pinch. In addition, since the time differences between the object sizes was very small, the proposed prosthesis had consistent performance regardless of the object size at the palmar pinch. In the case of tip pinch, it took average 3.7 seconds with normal hand and 3.94 second with our prosthesis. The difference between them were about 0.2 seconds, then our prosthesis had also similar performance at the tip pinch. However, the measured time increased relative to the object size. This is because the subject was hard to grasp the large cylinder

object by applying the appropriate force to the normal direction using only the tip of the distal phalanx. On the other hand, the subject could easily apply the force to the normal direction when the thin cylinder was grasped. The main reason of the tip pinch experiment was that the end effector of the proposed system was made to resemble the actual human fingertip by the silicon material. The direction of the applied the force depended on the shape of the fingertip and the prototype was designed to easily grasp the thin objects. By adjusting the shape of the fingertip, the grasping performance of the tip pinch could be similar regardless of the object sizes.

Grasp	Palmar pinch			Tip Pinch		
Size (mm)	Prosthesis		Difference (sec)	Prosthesis		Difference (sec)
	without (sec)	with (sec)		without (sec)	with (sec)	
5	3.34	3.78	0.44	3.49	3.60	0.11
10	3.59	4.07	0.48	3.69	3.85	0.16
15	3.42	3.84	0.42	3.74	4.10	0.36
20	3.45	3.99	0.53	3.87	4.21	0.34
Average	3.45	3.92	0.47	3.70	3.94	0.24
Success rate	20/20	20/20		20/20	19/20	

Table III.4 Result of grasping performance experiment

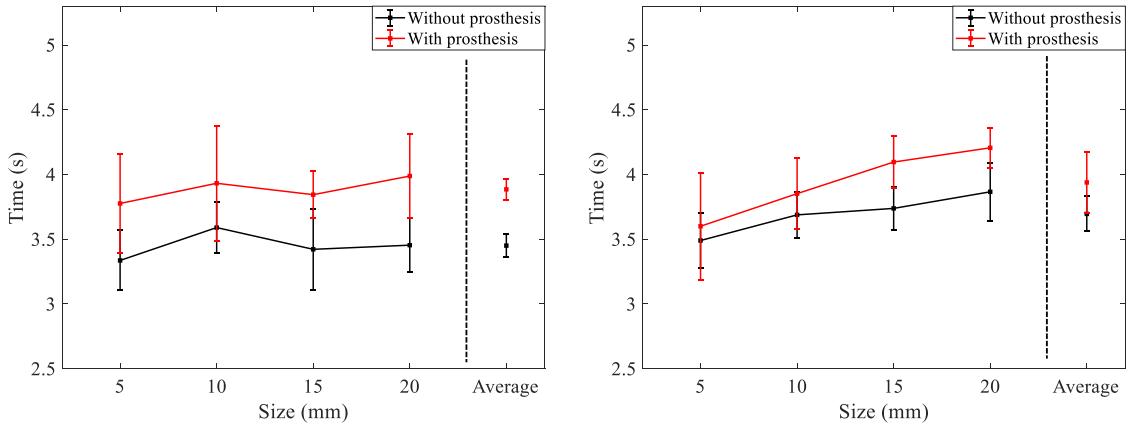

(a) Palmar pinch result

(b) Tip pinch result

Fig. III.32 Result of grasping performance experiment

IV. Conclusions

In this thesis, a design of a body-powered under-actuated prosthesis based on polar coordinate analysis was proposed for an index finger amputee. The prosthesis was designed to satisfy the following requirements: it should support the finger amputee to grasp and manipulate objects with a natural finger motion and should be of an appropriate size with respect to the aesthetic sense. Therefore, the under-actuation system by the serially connected incomplete four-bar mechanisms was proposed to realize the grasping motion, which generates PIP and DIP joint movements by the MCP joint of the amputee. The fingertip trajectory was considered as the representative factor of the natural finger motion and the new curve fitting method was proposed, based on the polar coordinate which covers the maximum flexion motion. The fingertip trajectory and anthropometric information of the subject were used to optimize the design variables of the system that satisfy the considerations of the practical finger prosthesis. The modular wearable interface was proposed for the user to wear the system easily and to manually align the system joint to the finger joint accurately.

The prototype was manufactured using the information from a normal subject before applying it to the actual finger amputee. Performance verification of trajectory generation and grasping performance was also conducted by the normal subject with and without the proposed finger prosthesis. The results showed that the proposed system could replace the finger in terms of grasping ability. The success rate of grasping the cylindrical objects with various radii (of 5 to 20 mm) was about 97 % (39/40), and the time difference between with the proposed system and without the system was very small; 0.2 ~ 0.4 seconds.

As a future work, we are planning to apply our proposed system to finger amputees. The prototype will be designed using the proposed design method according to individual requirements and practical issues will be considered to improve the proposed system by interacting with the finger amputees. Finally, the performance of grasping and manipulating the object will be verified experimentally.

REFERENCE

[1] K. Ziegler-Graham, E. J. MacKenzie, P. L. Ephraim, T. G. Travison, and R. Brookmeyer, "Estimating the prevalence of limb loss in the United States: 2005 to 2050," *Archives of physical medicine and rehabilitation,* vol. 89, no. 3, pp. 422-9, Mar, 2008.

[2] ' Healthcare Cost and Utilization Project, Nationwide Inpatient Sample (HCUP-NIS)'. [Online]. https://hcupnet.ahrq.gov [Accessed: 11-12 2018].

[3] D. P. Murphy, *Fundamentals of amputation care and prosthetics*, New York, USA: Demos Medical Publishing, 2013.

[4] A. G. Nerlich, A. Zink, U. Szeimies, and H. G. Hagedorn, "Ancient Egyptian prosthesis of the big toe," *The Lancet,* vol. 356, no. 9248, pp. 2176-2179, 2000.

[5] P. Hernigou, "Ambroise Paré IV: the early history of artificial limbs (from robotic to prostheses)," *International orthopaedics,* vol. 37, no. 6, pp. 1195-1197, 2013.

[6] M. Arazpour, M. A. Mardani, M. Ahmadi Bani, F. Zarezadeh, and S. W. Hutchins, "Design and fabrication of a finger prosthesis based on a new method of suspension," *Prosthetics and orthotics international,* vol. 37, no. 4, pp. 332-335, 2013.

[7] 'i-digits™ quantum'. [Online]. http://touchbionics.com/ [Accessed: 10-9 2018].

[8] 'Partial M-Finger'. [Online]. http://www.liberatingtech.com/ [Accessed: 10-8 2018].

[9] 'X-finger'. [Online]. https://www.x-finger.com [Accessed: 10-10 2018].

[10] 'The MCPDriver™'. [Online]. https://www.npdevices.com/ [Accessed: 10-12 2018].

[11] N. Dechev, W. L. Cleghorn, and S. Naumann, "Multiple finger, passive adaptive grasp prosthetic hand," *Mechanism and Machine Theory,* vol. 36, no. 10, pp. 1157-1173, Oct, 2001.

[12] B. Massa, S. Roccella, M. C. Carrozza, and P. Dario, "Design and development of an underactuated prosthetic hand." pp. 3374-3379.

[13] D. A. Neumann, *Kinesiology of the musculoskeletal system-e-book: foundations for rehabilitation*: Elsevier Health Sciences, 2013.

[14] J. Ponce, and B. Faverjon, "On computing three-finger force-closure grasps of polygonal objects," *IEEE Transactions on robotics automation,* vol. 11, no. 6, pp. 868-881, 1995.

[15] W. Park, K. Ro, S. Kim, and J. Bae, "A soft sensor-based three-dimensional (3-D) finger motion measurement system," *Sensors,* vol. 17, no. 2, pp. 420, 2017.

[16] M. C. Hume, H. Gellman, H. McKellop, and R. H. Brumfield Jr, "Functional range of motion of the joints of the hand," *The Journal of hand surgery,* vol. 15, no. 2, pp. 240-243, 1990.

[17] L.-C. Kuo, F.-C. Su, H.-Y. Chiu, and C.-Y. Yu, "Feasibility of using a video-based motion analysis system for measuring thumb kinematics," *Journal of Biomechanics,* vol. 35, no. 11, pp. 1499-1506, Nov, 2002.

[18] J. R. Cook, N. A. Baker, R. Cham, E. Hale, and M. S. Redfern, “Measurements of wrist and finger postures: a comparison of goniometric and motion capture techniques,” *Journal of applied biomechanics,* vol. 23, no. 1, pp. 70-78, Feb, 2007.

[19] G. D. Kessler, L. F. Hodges, and N. Walker, “Evaluation of the CyberGlove as a whole-hand input device,” *ACM Transactions on Computer-Human Interaction,* vol. 2, no. 4, pp. 263-283, 1995.

[20] J.-B. Chossat, Y. Tao, V. Duchaine, and Y.-L. Park, "Wearable soft artificial skin for hand motion detection with embedded microfluidic strain sensing." pp. 2568-2573.

[21] K. Ro, S. Kim, W. Park, and J. Bae, "Development of a wearable soft sensor system for measuring finger motions." pp. 549-554.

[22] Y. Park, J. Lee, and J. Bae, “Development of a wearable sensing glove for measuring the motion of fingers using linear potentiometers and flexible wires,” *IEEE Transactions on Industrial Informatics,* vol. 11, no. 1, pp. 198-206, 2015.

[23] J. Yang, H. Xie, and J. Shi, “A novel motion-coupling design for a jointless tendon-driven finger exoskeleton for rehabilitation,” *Mechanism and Machine Theory,* vol. 99, pp. 83-102, May, 2016.

[24] 'OptiTrack, Camera-Based Motion Capturing System'. [Online]. https://optitrack.com/ [Accessed: 11-16 2018].

[25] D. G. Kamper, E. G. Cruz, and M. P. Siegel, “Stereotypical fingertip trajectories during grasp,” *Journal of neurophysiology,* vol. 90, no. 6, pp. 3702-3710, 2003.

[26] T. Kline, D. Kamper, and B. Schmit, "Control system for pneumatically controlled glove to assist in grasp activities." pp. 78-81.

[27] B. Buchholz, T. J. Armstrong, and S. A. Goldstein, “Anthropometric data for describing the kinematics of the human hand,” *Ergonomics,* vol. 35, no. 3, pp. 261-273, Mar, 1992.

[28] P. Hahn, H. Krimmer, A. Hradetzky, and U. Lanz, “Quantitative-Analysis of the Linkage between the Interphalangeal Joints of the Index Finger - an in-Vivo Study,” *Journal of Hand Surgery-British and European Volume,* vol. 20b, no. 5, pp. 696-699, Oct, 1995.

[29] J. Wang, J. Li, Y. Zhang, and S. Wang, "Design of an exoskeleton for index finger rehabilitation." pp. 5957-5960.

[30] J. N. Ingram, K. P. Körding, I. S. Howard, and D. M. Wolpert, “The statistics of natural hand movements,” *Experimental brain research,* vol. 188, no. 2, pp. 223-236, 2008.

[31] D. D. Didrick, "Articulated artificial finger assembly," Google Patents, 2005.

[32] 'C40, Laser cutting machine'. [Online]. http://www.coryart.co.kr [Accessed: 11-20 2018].

[33] M. A. Srinivasan, and C. Basdogan, “Haptics in virtual environments: Taxonomy, research status, and challenges,” *Computers & Graphics,* vol. 21, no. 4, pp. 393-404, 1997.

[34] T. Feix, J. Romero, H. B. Schmiedmayer, A. M. Dollar, and D. Kragic, “The GRASP Taxonomy of Human Grasp Types,” *Ieee Transactions on Human-Machine Systems,* vol. 46, no. 1, pp. 66-77, Feb,

2016.

[35] C. M. Light, P. H. Chappell, and P. J. Kyberd, “Establishing a standardized clinical assessment tool of pathologic and prosthetic hand function: normative data, reliability, and validity,” *Archives of physical medicine and rehabilitation,* vol. 83, no. 6, pp. 776-83, Jun, 2002.

Acknowledgements

I would like to appreciate all the members of BIRC lab for their great support.

First, I want to express deep gratitude to Professor Joonbum Bae for guiding and teaching me. Without his continues guide, this study might not be completed. I am honored that I can study and learn under the Professor Joonbum Bae.

Also, I appreciate to my group leader Yeongyu Park. Because of his leadership I could learn lots of things from him, and my group members, Inseong Jo and Jeongsoo Lee, give always helpful ideas of the research. That comments inspired me a lot. Even though other members (Dr. Ba, Yeongtae Jung, Jihoon Kim, Suin Kim, Sungman Park, Hoyeon Yeom, Wookeun Park, Minhyuk Lee, Kyutaek Han, Junsoo Kim, Dahee Jung, Dongyoung Lee, Sungmin Seo, Heeyeop Kim and Jeongsoon Hong) did not work with me, it was a pleasure being with them and I will always remember our time together.

I always thank my family who have supported me through my life. Their cheer and belief always made me to be encouraged. Especially, without my fiancé, I could not enjoy the graduate school life.

Lastly, thanks to people who I did not mention. I will remember all their support.